
SMA-DP: Spectral Memory-Aware Differential Privacy for Deep Learning

Mohammad Partohaghighi

Department of Electrical Engineering and Computer Science
University of California, Merced
Merced, CA, USA
mpartohaghighi@ucmerced.edu

Roummel P. Marcia

Department of Applied Mathematics
University of California, Merced
Merced, CA, USA
rmarcia@ucmerced.edu

Abstract

Differentially private stochastic gradient descent (DP-SGD) enables private deep learning through per-example clipping and calibrated Gaussian noise, but the resulting updates can be high-variance and may degrade utility, especially on more challenging datasets. We propose **SMA-DP-SGD**, a **Spectral Memory-Aware Differentially Private Stochastic Gradient Descent** method that augments DP-SGD with a fractional memory branch constructed only from previously privatized noisy releases. The method uses WeightWatcher-inspired power-law spectral exponents as group-wise reliability signals to adapt the decay and effective depth of memory; in our experiments, the group-wise formulation is instantiated layer-wise. Private-history alignment, norm matching, and warm-up activation further stabilize the memory contribution. The privacy structure remains transparent: conditioned on the private release history, the memory branch is fixed, and the only newly data-dependent term is the current clipped sum scaled by a fixed coefficient β . Thus, SMA-DP-SGD preserves a clean conditional sensitivity structure and exactly recovers standard group-wise DP-SGD when $\beta = 1$. Experiments on CIFAR-100, CIFAR-10, and MNIST show that SMA-DP-SGD achieves competitive or superior accuracy compared with several DP optimization baselines, with the strongest gains appearing on the more challenging CIFAR-100 and CIFAR-10 settings. Ablations on CIFAR-10 show that the mixing parameter β controls the privacy–utility trajectory, while spectral and memory diagnostics confirm that the method maintains a controlled short-to-moderate effective memory depth and a small memory-branch ratio. Runtime analysis shows that this spectral memory mechanism introduces additional computational overhead, about $2.94\times$ DP-SGD in our CIFAR-10 implementation, highlighting a practical trade-off between adaptive private memory and computational cost.

Keywords: Differential Privacy; DP-SGD; Private Deep Learning; Fractional Memory Optimization; Spectral Diagnostics; WeightWatcher; Heavy-Tailed Self-Regularization; Private Release History; Adaptive Memory Tempering; Privacy–Utility Trade-off

1 Introduction

Deep neural networks are increasingly trained on sensitive data, including medical records, genomic profiles, user behavior, financial transactions, and personal-device data. Differential privacy (DP) provides a rigorous framework for limiting the influence of any individual training example on the learned model Dwork et al. [2006], Dwork and Roth [2014], Partohaghighi et al. [2026c]. In private deep learning, differentially private stochastic gradient descent (DP-SGD) has become a standard workhorse: it clips per-example gradients and adds calibrated Gaussian noise before updating the model Abadi et al. [2016]. This mechanism has enabled private training in centralized, federated, and data-sensitive learning settings McMahan et al. [2018], Papernot et al. [2018]. However, the same clipping and noise that provide privacy also perturb the optimization signal, often increasing variance, slowing convergence, and reducing utility.

A substantial body of work has improved private training through sharper privacy accounting, subsampling analyses, adaptive clipping, transfer learning, and scaling strategies Mironov [2017], Wang et al. [2019], Bu et al. [2020], Andrew et al. [2021], Tramèr and Boneh [2021], De et al. [2022]. These developments have significantly improved the practicality of DP deep learning, yet noisy private optimization remains challenging. In particular, DP-SGD typically relies heavily on the current noisy clipped gradient. When the privacy budget is tight, this current update can be a high-variance estimate of the underlying optimization direction, making training sensitive to clipping norms, noise multipliers, learning rates, and model scale Bassily et al. [2014], De et al. [2022].

Private optimization need not be memoryless. Classical stochastic optimization already exploits historical information through momentum, acceleration, adaptive preconditioning, and adaptive moments Robbins and Monro [1951], Polyak [1964], Nesterov [1983], Duchi et al. [2011], Kingma and Ba [2015]. The same principle is compelling under DP: previous noisy private releases may still contain useful directional information about the optimization trajectory. Discarding all historical information forces training to rely primarily on the current noisy clipped gradient, which can amplify variance and slow convergence. At the same time, memory must be introduced carefully under DP. Raw historical gradients remain data-dependent, and current-gradient-dependent memory gates can create additional data-dependent pathways that obscure the sensitivity of the current query. This motivates a privacy-compatible memory principle: *historical information should enter the private update only through quantities that have already been privatized.*

Fractional calculus provides a principled framework for modeling memory-dependent and nonlocal dynamics through power-law historical kernels Podlubny [1999], Kilbas et al. [2006], Diethelm [2010], Meerschaert and Sikorskii [2012], West [2014]. Unlike short-horizon exponential moving averages, fractional-order memory kernels can represent long-range temporal dependence, making them a natural mechanism for aggregating optimization signals across multiple steps. In a DP setting, however, the historical kernel should not be applied to raw gradients. Instead, the memory source must be the *private release history*: the sequence of previously privatized noisy releases. This preserves the intended historical structure while keeping the memory branch compatible with privacy accounting.

A second challenge is that memory should not be blind or uniform across layers. A fixed memory horizon treats all layers as equally reliable, even though different layers may exhibit different training states, spectral organization, stability, noise sensitivity, and generalization behavior. In non-private deep learning, the spectra of weight matrices have been widely studied as indicators of optimization geometry, sharpness, capacity, and generalization Bartlett et al. [2017], Neyshabur et al. [2017], Keskar et al. [2017], Pennington and Worah [2017], Ghorbani et al. [2019], Foret et al. [2021]. These observations suggest that layer-wise spectral structure can provide information about how aggressively each layer should retain or forget historical signals.

We therefore draw on Heavy-Tailed Self-Regularization (HT-SR) and WeightWatcher-style spectral diagnostics. This line of work analyzes the empirical spectral density of trained weight matrices and fits power-law tails to layer spectra Martin and Mahoney [2019, 2021]. Martin, Peng, and Mahoney showed that such power-law spectral metrics can diagnose quality trends of pretrained neural networks, including settings where training and testing data are unavailable Martin et al. [2021]. In this paper, we use the resulting spectral exponent not as a privacy mechanism, and not as a universal certificate of layer quality, but as a layer-wise reliability heuristic for controlling how

quickly private memory should decay. This use is motivated by spectral diagnostics and evaluated empirically through ablations.

Despite progress in DP optimization, fractional memory modeling, and spectral diagnostics, their intersection remains underexplored. Existing DP optimizers primarily focus on clipping, noise calibration, privacy accounting, adaptive moments, preconditioning, and training stabilization. Fractional methods provide memory models, but are generally not designed around DP-SGD conditional sensitivity. WeightWatcher and HT-SR provide layer-wise spectral diagnostics, but are typically used for model diagnosis rather than as control signals for privacy-compatible memory. To our knowledge, there has not been a systematic study of a DP-SGD extension that simultaneously combines private release-history memory, fractional power-law weighting, layer-wise spectral reliability, clean conditional sensitivity analysis, and exact reduction to DP-SGD.

We propose **SMA-DP-SGD**, a **Spectral Memory-Aware Differentially Private Stochastic Gradient Descent** method. At each private step, SMA-DP-SGD constructs a fractional memory branch for each parameter group from the private release history, i.e., previously privatized noisy gradient releases. The formulation is group-wise and general; in our experiments, each trainable layer is instantiated as one group, so the mechanism operates layer-wise. A WeightWatcher-inspired power-law exponent provides a group-specific reliability signal that controls spectral tempering: groups with favorable spectral organization retain longer effective memory, whereas groups outside the chosen reliability range forget older releases more aggressively. The memory contribution is further stabilized using private-history alignment, norm matching, and warm-up activation. A fixed mixing coefficient controls the interpolation between the current clipped update and the memory branch; when this coefficient disables the memory contribution, SMA-DP-SGD exactly reduces to standard group-wise DP-SGD.

The privacy argument is intentionally transparent. The memory branch is computed only from the prior private release history, and is therefore fixed after conditioning on that history. Consequently, the only newly data-dependent component of the current query is the scaled clipped gradient contribution. This yields a clean group-wise conditional sensitivity structure while avoiding the reuse of raw historical gradients. The formal full-step privacy guarantee uses a conservative joint accountant across parameter groups, while marginal noise-to-sensitivity ratios are used only for group-wise diagnostic interpretation.

Our contributions are summarized as follows:

- We introduce SMA-DP-SGD, a DP-SGD extension that injects fractional memory using previous noisy private releases rather than raw historical gradients.
- We use WeightWatcher-inspired spectral exponents as layer-wise reliability signals to adapt memory decay and effective memory depth.
- We provide a clean conditional sensitivity structure and show that SMA-DP-SGD exactly recovers standard group-wise DP-SGD when the memory contribution is disabled.
- We empirically evaluate the method against DP optimization baselines and through ablations over spectral intervals, effective memory depth, memory ratios, fixed mixing coefficient, shared fractional order, shared memory window, and shuffled spectral assignments.

The remainder of this paper is organized as follows. Section 2 reviews related work on differentially private optimization, fractional memory modeling, and spectral diagnostics. Section 3 presents SMA-DP-SGD, including the private-release-history memory construction, spectral tempering, and group-wise update rule. Section 4 describes the experimental setup and reports the main empirical results, ablation studies, spectral diagnostics, and runtime comparison. Section 6 discusses broader impacts. Section 5 concludes the paper and summarizes limitations and future directions. Additional experimental results and diagnostics are provided in Appendix A, and the full theoretical analysis is provided in Appendix B.

2 Related Work

Differentially private deep learning. Differential privacy provides a formal framework for limiting the influence of individual training examples on the output of a learning algorithm Dwork et al. [2006], Dwork and Roth [2014]. DP-SGD has become the standard optimization mechanism for

private deep learning by combining per-example gradient clipping with calibrated Gaussian perturbations Abadi et al. [2016]. Subsequent work has improved the practicality of private training through refined privacy accounting, subsampled RDP analysis, Gaussian DP, adaptive clipping, transfer learning, and large-scale private training strategies Mironov [2017], Wang et al. [2019], Bu et al. [2020], Andrew et al. [2021], Tramèr and Boneh [2021], De et al. [2022]. These methods primarily address the privacy–utility trade-off through accounting, clipping, noise calibration, scaling, or optimizer design. In contrast, SMA-DP-SGD focuses on a complementary question: how to inject useful historical information into private optimization without reusing raw historical gradients or obscuring the sensitivity of the current query.

Memory and adaptive optimization. Historical information is central to stochastic optimization. Classical momentum and accelerated methods exploit past directions to stabilize and speed up optimization, while adaptive methods such as AdaGrad and Adam use accumulated gradient statistics to rescale updates Robbins and Monro [1951], Polyak [1964], Nesterov [1983], Duchi et al. [2011], Kingma and Ba [2015]. Private optimizers can also contain optimizer-state memory, but under differential privacy this memory must be handled carefully because raw gradients and current-batch-dependent gates can introduce additional data-dependent pathways. SMA-DP-SGD differs from standard momentum or Adam-style memory by constructing its memory branch only from previously privatized noisy releases. This private-release-history construction allows historical information to influence optimization while preserving a clean conditional sensitivity structure.

Fractional memory modeling. Fractional calculus provides a principled framework for modeling nonlocal and memory-dependent dynamics through power-law historical kernels Podlubny [1999], Kilbas et al. [2006], Diethelm [2010], Meerschaert and Sikorskii [2012], West [2014]. Compared with short-horizon exponential moving averages, fractional kernels offer a natural mechanism for representing longer-range temporal dependence. SMA-DP-SGD uses this perspective to define a tempered fractional memory state over previous private releases. The key distinction in our setting is privacy compatibility: the fractional kernel is applied only to already privatized releases, rather than to raw historical gradients.

Spectral diagnostics and Heavy-Tailed Self-Regularization. The spectra of neural-network weight matrices have been studied in connection with capacity, optimization geometry, sharpness, and generalization Bartlett et al. [2017], Neyshabur et al. [2017], Keskar et al. [2017], Pennington and Worah [2017], Ghorbani et al. [2019], Foret et al. [2021]. Heavy-Tailed Self-Regularization and WeightWatcher-style diagnostics analyze the empirical spectral density of trained weight matrices and fit power-law tails to their eigenvalue distributions Martin and Mahoney [2019, 2021]. Martin, Peng, and Mahoney showed that power-law spectral metrics can diagnose quality trends of pretrained neural networks even without access to training or testing data Martin et al. [2021]. More recent work has also used WeightWatcher-style spectral diagnostics as control or stability signals in privacy-preserving training and machine unlearning: spectral indicators have been used to adapt gradient-clipping thresholds in differentially private training, and layer-wise heavy-tailed spectral diagnostics have been used to reweight unlearning updates according to statistical roughness Partoghghi et al. [2026a,b]. Our work uses these spectral diagnostics in a different role: the power-law exponent is treated as a layer-wise reliability heuristic for controlling the decay of private fractional memory. We do not use the spectral exponent as a privacy mechanism or as a universal certificate of layer quality; instead, it modulates how aggressively each layer forgets older private releases.

Positioning of SMA-DP-SGD. SMA-DP-SGD combines three ideas that have largely been studied separately: differentially private optimization, fractional memory modeling, and spectral diagnostics. Existing DP methods typically focus on clipping, noise, privacy accounting, adaptive optimizers, or scaling strategies; fractional methods provide memory kernels but are not designed around DP-SGD sensitivity; and WeightWatcher-style diagnostics are usually used for model analysis rather than as control signals inside private optimization. SMA-DP-SGD bridges these directions by building a fractional memory branch from the private release history and adapting its decay using layer-wise spectral reliability, while retaining an exact reduction to standard group-wise DP-SGD when $\beta = 1$.

3 Methodology

We propose **SMA-DP-SGD**, a **Spectral Memory-Aware Differentially Private Stochastic Gradient Descent** method. SMA-DP-SGD extends DP-SGD with a fractional memory branch computed for each predefined parameter group from the *private release history*, i.e., the sequence of previously privatized noisy gradient releases. The memory branch is regulated by spectral tempering, private-history alignment, warm-up activation, and norm matching.

We formulate SMA-DP-SGD for generic parameter groups and instantiate each trainable layer as one group in our experiments, allowing the spectral memory mechanism to operate layer-wise. This distinction is important: the privacy analysis is group-wise and applies to any predefined partition of the trainable parameters, while the experimental implementation uses the natural layer-wise partition induced by convolutional and linear layers.

The key design principle is that, at private step t , the memory branch is constructed only from previously privatized releases and public hyperparameters. Consequently, conditioned on the prior private release history, the memory contribution is fixed, and the only newly data-dependent component of the query is the current clipped subsampled sum scaled by a fixed coefficient β . This structure preserves an exact reduction to standard DP-SGD when $\beta = 1$, while yielding a clean conditional sensitivity analysis.

3.1 Problem setup

Let $D = \{x_i\}_{i=1}^N$ denote the training dataset and let $\ell(\theta; x_i)$ be the loss of a model with trainable parameter vector θ . We partition the trainable parameters into G predefined groups, $\theta = (\theta^{(1)}, \theta^{(2)}, \dots, \theta^{(G)})$, where $g \in \{1, \dots, G\}$ indexes a parameter group.

This group-wise formulation is general: a group may correspond to a layer, a block, a module, or any predefined subset of trainable parameters. In our experiments, we use the layer-wise instantiation, where each trainable convolutional or linear layer is treated as one group. Therefore, all group-wise quantities, including $s_t^{(g)}$, $C^{(g)}$, $\rho_t^{(g)}$, $\lambda_t^{(g)}$, $\nu_{t-1}^{(g)}$, $\Gamma_t^{(g)}$, and $\Psi_t^{(g)}$, become layer-wise quantities in the experimental implementation.

At private step t , a Poisson subsample $S_t \subseteq D$ is drawn with sampling probability q , where q controls the expected lot size $L = qN$. For each sampled example $x_i \in S_t$, the group-wise per-example gradient is $g_t^{(g)}(x_i) = \nabla_{\theta^{(g)}} \ell(\theta_t; x_i)$. We apply group-wise clipping,

$$\bar{g}_t^{(g)}(x_i) = \frac{g_t^{(g)}(x_i)}{\max\left(1, \|g_t^{(g)}(x_i)\|_2 / C^{(g)}\right)}, \quad \|\bar{g}_t^{(g)}(x_i)\|_2 \leq C^{(g)},$$

where $C^{(g)}$ controls the group-wise sensitivity of the clipped contribution. We define the clipped subsampled sum $s_t^{(g)} = \sum_{x_i \in S_t} \bar{g}_t^{(g)}(x_i)$. For each group g , SMA-DP-SGD maintains the private release history $\mathcal{H}_t^{(g)} = \{\tilde{s}_0^{(g)}, \tilde{s}_1^{(g)}, \dots, \tilde{s}_{t-1}^{(g)}\}$, where $\tilde{s}_r^{(g)}$ is the noisy private release produced at step $r < t$. The history is empty at $t = 0$.

All memory-dependent quantities at step t are computed from $\mathcal{H}_t^{(g)}$, the model state induced by previous private updates, and public hyperparameters. The method does not use raw historical gradients, current unclipped gradients, or the current clipped sum to construct the memory branch. Hence, after conditioning on $\mathcal{H}_t^{(g)}$, the memory contribution is fixed. The spectral reliability signal is motivated by Heavy-Tailed Self-Regularization and WeightWatcher-style diagnostics, which analyze the empirical spectral density of layer weight matrices and fit power-law tails to their eigenvalue distributions. Prior work has shown that such power-law spectral metrics can diagnose quality trends in pretrained neural networks, including settings where training or testing data are unavailable Martin et al. [2021]. In SMA-DP-SGD, these diagnostics are not used as privacy mechanisms; rather, they provide group-wise reliability signals for controlling the decay of private memory. Under the layer-wise instantiation used in our experiments, these reliability signals are computed per trainable layer.

For spectral diagnostics, a group is assumed to contain a matrix-shaped trainable weight tensor, or a tensor that can be reshaped into a two-dimensional matrix, as in convolutional and linear layers.

Following WeightWatcher-style spectral diagnostics Martin et al. [2021], for a matrix-shaped group with weight matrix $W_t^{(g)}$, we form $X_t^{(g)} = (W_t^{(g)})^\top W_t^{(g)}$. For convolutional kernels, the kernel tensor is first reshaped into an appropriate two-dimensional matrix before forming the corresponding spectral matrix. Let $\{\lambda_i^{(g)}\}$ denote the eigenvalues of $X_t^{(g)}$. We estimate a WeightWatcher-style power-law exponent $\rho_t^{(g)}$, which serves as a group-wise spectral reliability signal, by fitting the upper tail of the empirical eigenvalue distribution, $p(\lambda) \propto \lambda^{-\rho_t^{(g)}}$. We use the notation $\rho_t^{(g)}$, rather than the conventional power-law symbol α , to avoid conflict with the fractional memory order α .

The exponent $\rho_t^{(g)}$ is computed from the current model state θ_t , which is induced by previous private releases. Thus, conditioned on the prior private release history and public hyperparameters, $\rho_t^{(g)}$ is fixed for the current query. Consequently, the spectral tempering mechanism affects only the already-determined memory branch and does not introduce additional current-batch dependence.

Motivated by the HT-SR/WeightWatcher interpretation, we treat intermediate power-law exponent ranges as favorable spectral-reliability regions. Let $I_\rho = [\rho_{\min}, \rho_{\max}]$ denote the spectral reliability interval used to decide whether a group should retain longer memory or forget older releases more aggressively. This interval is a tunable design choice rather than a universal criterion for layer quality. To measure how far the current spectral exponent lies outside the reliability interval, define

$$d_t^{(g)}(I_\rho) = \max\left(0, \rho_{\min} - \rho_t^{(g)}, \rho_t^{(g)} - \rho_{\max}\right).$$

Equivalently, with $m_\rho = (\rho_{\min} + \rho_{\max})/2$ and $h_\rho = (\rho_{\max} - \rho_{\min})/2$, the same deviation can be written compactly as

$$d_t^{(g)}(I_\rho) = \max\left(0, |\rho_t^{(g)} - m_\rho| - h_\rho\right).$$

Thus, $d_t^{(g)}(I_\rho) = 0$ whenever $\rho_t^{(g)} \in I_\rho$, and otherwise measures the distance of $\rho_t^{(g)}$ from the closest endpoint of the reliability interval. In the default configuration, we use $I_\rho^* = [2, 6]$, corresponding to $m_\rho = 4$ and $h_\rho = 2$. We do not assume that this interval is universally optimal; its role is to define the reliability range used by the spectral tempering mechanism.

The spectral deviation controls the group-wise tempering coefficient

$$\lambda_t^{(g)}(I_\rho) = 1 - \exp\left(-c_\lambda d_t^{(g)}(I_\rho)\right), \quad c_\lambda > 0,$$

where c_λ controls how strongly spectral deviation is converted into memory tempering. When $\rho_t^{(g)} \in I_\rho$, the deviation is zero and $\lambda_t^{(g)}(I_\rho) = 0$, so the corresponding group retains longer effective memory. When $\rho_t^{(g)} \notin I_\rho$, the deviation is positive and $\lambda_t^{(g)}(I_\rho) > 0$, so older private releases are down-weighted more aggressively. In this work, SMA-DP-SGD uses a shared memory window K , which sets the maximum number of previous private releases used by the memory branch, and a shared fractional order $\alpha \in (0, 1]$, which controls the power-law decay of the fractional memory kernel, across all parameter groups. Group-wise adaptivity enters through the spectral tempering coefficient $\lambda_t^{(g)}(I_\rho)$, which depends on the group-wise spectral exponent $\rho_t^{(g)}$. At step t , the number of available memory terms is $M_t = \min(K - 1, t)$. For $j = 1, \dots, M_t$, define

$$a_{t,j}^{(g)} = (j + 1)^{\alpha-1} \exp\left(-\lambda_t^{(g)}(I_\rho)j\right) \quad \text{and} \quad \hat{a}_{t,j}^{(g)} = \frac{a_{t,j}^{(g)}}{\sum_{\ell=1}^{M_t} a_{t,\ell}^{(g)}}.$$

The private fractional memory state, $\nu_{t-1}^{(g)}$, and effective memory depth, $D_{\text{eff},t}^{(g)}$, are given by

$$\nu_{t-1}^{(g)} = \sum_{j=1}^{M_t} \hat{a}_{t,j}^{(g)} \tilde{s}_{t-j}^{(g)} \quad \text{and} \quad D_{\text{eff},t}^{(g)} = \sum_{j=1}^{M_t} j \hat{a}_{t,j}^{(g)},$$

respectively. If $M_t = 0$, then $\nu_{t-1}^{(g)} = 0$. The effective memory depth $D_{\text{eff},t}^{(g)}$ summarizes how far into the private release history the group effectively looks. Although K and α are shared, the normalized weights $\hat{a}_{t,j}^{(g)}$ and the resulting memory depth remain group-wise because they depend on the group-wise tempering coefficient $\lambda_t^{(g)}(I_\rho)$. Smaller tempering values generally yield longer

SMA-DP-SGD: Spectral Memory-Aware Differentially Private SGD

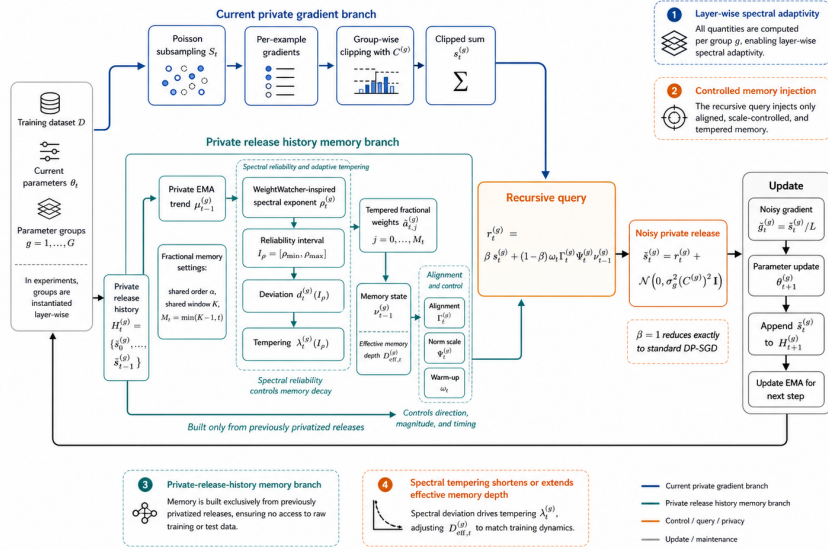


Figure 1: Overview of SMA-DP-SGD, combining a current private gradient branch with a spectrally tempered private-release-history memory branch.

effective memory, whereas larger values shorten the memory horizon. Historical memory can be harmful when it points in a direction inconsistent with the recent private optimization trend. To suppress stale or contradictory memory, SMA-DP-SGD constructs a private exponential moving average trend from previous releases:

$$\mu_{t-1}^{(g)} = \gamma_{\text{ema}} \tilde{s}_{t-1}^{(g)} + (1 - \gamma_{\text{ema}}) \mu_{t-2}^{(g)}, \quad \gamma_{\text{ema}} \in (0, 1],$$

where γ_{ema} controls the recency of the private EMA trend, with larger values emphasizing more recent private releases. We initialize $\mu_0^{(g)} = \tilde{s}_0^{(g)}$. At $t = 0$, no previous release exists, and the memory branch is set to zero.

The private-history alignment gate is

$$\Gamma_t^{(g)} = \max \left(0, \frac{\langle \mu_{t-1}^{(g)}, \nu_{t-1}^{(g)} \rangle}{\|\mu_{t-1}^{(g)}\|_2 \|\nu_{t-1}^{(g)}\|_2 + \epsilon} \right),$$

where $\epsilon > 0$ is a numerical stability constant that prevents division by very small norms. The gate suppresses memory directions that are not aligned with the recent private trend. Even aligned memory may have an inappropriate magnitude, so we use the norm-matching scale

$$\Psi_t^{(g)} = \min \left(\xi_{\max}, \frac{\|\mu_{t-1}^{(g)}\|_2}{\|\nu_{t-1}^{(g)}\|_2 + \epsilon} \right), \quad \xi_{\max} > 0,$$

where ξ_{\max} caps memory amplification induced by norm matching. Both $\Gamma_t^{(g)}$ and $\Psi_t^{(g)}$ are computed only from previous private releases. Thus, the memory contribution is directionally filtered and scale-controlled before entering the private query. Algorithm 1 summarizes SMA-DP-SGD. The method uses a deterministic warm-up coefficient $\omega_t = 1 - \exp(-t/\tau_{\text{warm}})$, where $\tau_{\text{warm}} > 0$ controls how quickly the memory branch becomes active, and a fixed current-memory mixing coefficient $\beta \in (0, 1]$, which controls the interpolation between the current clipped update and the private-release-history memory branch. The recursive query for group g is

$$r_t^{(g)} = \beta s_t^{(g)} + (1 - \beta) \omega_t \Gamma_t^{(g)} \Psi_t^{(g)} \nu_{t-1}^{(g)}.$$

Equivalently, $r_t^{(g)} = \beta s_t^{(g)} + b_t^{(g)}(\mathcal{H}_t^{(g)})$, where $b_t^{(g)}(\mathcal{H}_t^{(g)})$ is the memory branch computed from the prior private release history. The case $\beta = 1$ removes the memory branch and recovers standard group-wise DP-SGD.

Algorithm 1 SMA-DP-SGD with Private Release-History Memory

Require: Dataset D , loss $\ell(\theta; x)$
Require: Predefined parameter groups $\theta = (\theta^{(1)}, \dots, \theta^{(G)})$, instantiated as trainable layers in the experiments
Require: Sampling rate q , learning rate η , clipping norms $C^{(g)}$, noise multipliers σ_g
Require: Shared memory window K , shared fractional order α , fixed mixing coefficient $\beta \in (0, 1]$
Require: Spectral interval $I_\rho = [\rho_{\min}, \rho_{\max}]$, tempering constant c_λ
Require: EMA coefficient γ_{ema} , warm-up scale τ_{warm} , norm cap ξ_{max} , stability constant $\epsilon > 0$

- 1: Initialize θ_0 , histories $\mathcal{H}_0^{(g)} \leftarrow \emptyset$, and trends $\mu_{-1}^{(g)} \leftarrow 0$ for all g
- 2: **for** $t = 0, \dots, T - 1$ **do**
- 3: Draw Poisson subsample S_t with probability q
- 4: Set $\omega_t \leftarrow 1 - \exp(-t/\tau_{\text{warm}})$ and $M_t \leftarrow \min(K - 1, t)$
- 5: **for** $g = 1, \dots, G$ **do**
- 6: Compute per-example gradients, clip them at $C^{(g)}$, and form $s_t^{(g)} = \sum_{x_i \in S_t} \bar{g}_t^{(g)}(x_i)$
- 7: **if** $t = 0$ **then**
- 8: Set $\nu_{t-1}^{(g)} \leftarrow 0$, $\Gamma_t^{(g)} \leftarrow 0$, and $\Psi_t^{(g)} \leftarrow 0$
- 9: **else**
- 10: Estimate $\rho_t^{(g)}$ from the matrix-shaped weight tensor of group g , when applicable
- 11: Compute $d_t^{(g)}(I_\rho) \leftarrow \max(0, \rho_{\min} - \rho_t^{(g)}, \rho_t^{(g)} - \rho_{\max})$
- 12: Compute $\lambda_t^{(g)}(I_\rho) \leftarrow 1 - \exp(-c_\lambda d_t^{(g)}(I_\rho))$
- 13: For $j = 1, \dots, M_t$, compute $a_{t,j}^{(g)} \leftarrow (j+1)^{\alpha-1} \exp(-\lambda_t^{(g)}(I_\rho)j)$ and $\hat{a}_{t,j}^{(g)} \leftarrow a_{t,j}^{(g)} / \sum_{\ell=1}^{M_t} a_{t,\ell}^{(g)}$
- 14: Construct $\nu_{t-1}^{(g)} \leftarrow \sum_{j=1}^{M_t} \hat{a}_{t,j}^{(g)} \tilde{s}_{t-j}^{(g)}$
- 15: Compute $\Gamma_t^{(g)} \leftarrow \max\left(0, \frac{\langle \mu_{t-1}^{(g)}, \nu_{t-1}^{(g)} \rangle}{\|\mu_{t-1}^{(g)}\|_2 \|\nu_{t-1}^{(g)}\|_2 + \epsilon}\right)$
- 16: Compute $\Psi_t^{(g)} \leftarrow \min\left(\xi_{\text{max}}, \frac{\|\mu_{t-1}^{(g)}\|_2}{\|\nu_{t-1}^{(g)}\|_2 + \epsilon}\right)$
- 17: **end if**
- 18: Form $r_t^{(g)} \leftarrow \beta s_t^{(g)} + (1 - \beta)\omega_t \Gamma_t^{(g)} \Psi_t^{(g)} \nu_{t-1}^{(g)}$
- 19: Release $\tilde{s}_t^{(g)} \leftarrow r_t^{(g)} + \mathcal{N}(0, \sigma_g^2 (C^{(g)})^2 I)$
- 20: Update $\theta_{t+1}^{(g)} \leftarrow \theta_t^{(g)} - \eta \tilde{s}_t^{(g)} / L$
- 21: Append $\tilde{s}_t^{(g)}$ to $\mathcal{H}_{t+1}^{(g)}$
- 22: Update $\mu_t^{(g)} \leftarrow \tilde{s}_0^{(g)}$ if $t = 0$, otherwise $\mu_t^{(g)} \leftarrow \gamma_{\text{ema}} \tilde{s}_t^{(g)} + (1 - \gamma_{\text{ema}}) \mu_{t-1}^{(g)}$
- 23: **end for**
- 24: **end for**
- 25: **return** θ_T

The private release is $\tilde{s}_t^{(g)} = r_t^{(g)} + Z_t^{(g)}$, with $Z_t^{(g)} \sim \mathcal{N}(0, \sigma_g^2 (C^{(g)})^2 I)$, where σ_g controls the Gaussian noise strength for group g . The noisy gradient estimate is $\tilde{g}_t^{(g)} = \tilde{s}_t^{(g)} / L$, and the group-wise parameter update is $\theta_{t+1}^{(g)} = \theta_t^{(g)} - \eta \tilde{g}_t^{(g)}$. After the update, $\tilde{s}_t^{(g)}$ is appended to $\mathcal{H}_{t+1}^{(g)}$, and the private EMA trend is updated for the next step. Figure 1 summarizes the SMA-DP-SGD workflow, where the current clipped private update is combined with a spectrally tempered memory branch built from previously privatized releases.

4 Experiment

We evaluate SMA-DP-SGD on CIFAR-10 and CIFAR-100 Krizhevsky [2009] and MNIST LeCun et al. [1998] against representative differentially private optimization baselines, including DP-SGD, DP-Adam, DP-AdamW, DP-IS, DP-SAM, DP-SAT, and DP-Adam-AC. The main experimental section reports the cross-dataset utility comparison, while additional ablations, stage-wise spectral diagnostics, final-accuracy statistics, marginal privacy-cost diagnostics, spectral-interval sensitivity analyses, and runtime comparisons are provided in Appendix A.

4.1 Cross-Dataset Accuracy Comparison under Differential Privacy

As shown in Fig. 2, SMA-DP-SGD exhibits strong and stable performance across CIFAR-100, CIFAR-10, and MNIST. On CIFAR-100, which is the most challenging benchmark among the three due to its larger number of classes and higher inter-class similarity, SMA-DP-SGD achieves the highest final test accuracy among the compared methods. This suggests that the proposed spectral memory-aware mechanism can improve learning under noisy private gradients, especially in more complex classification settings where standard DP optimizers may suffer from unstable or under-optimized convergence.

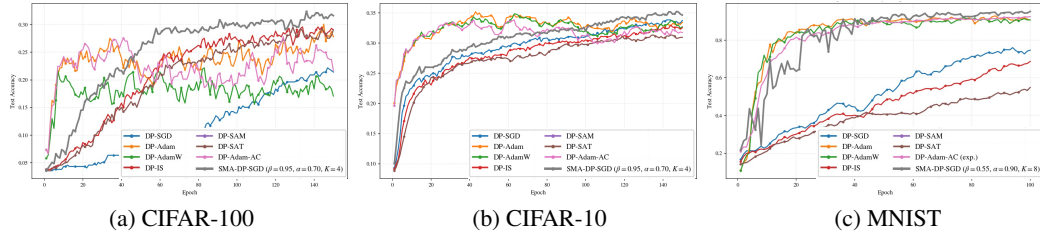


Figure 2: Cross-dataset comparison of test accuracy versus training epoch for differentially private optimizers on (a) CIFAR-100, (b) CIFAR-10, and (c) MNIST. SMA-DP-SGD is compared against representative DP optimization baselines under matched experimental settings.

On CIFAR-10, most adaptive DP optimizers reach relatively similar accuracy levels after the early training phase. Nevertheless, SMA-DP-SGD remains highly competitive throughout training and achieves one of the strongest final accuracy values. This indicates that the proposed method does not merely benefit from dataset-specific behavior on CIFAR-100, but also generalizes well to moderately complex image classification tasks.

For MNIST, several adaptive methods, including DP-Adam, DP-AdamW, DP-SAM, and DP-SAT, quickly reach high accuracy due to the relative simplicity of the dataset. SMA-DP-SGD also achieves high final accuracy and remains close to the best-performing methods. This result indicates that the proposed method preserves stable learning behavior on simpler datasets while offering stronger advantages on more challenging benchmarks.

5 Conclusion

This paper introduced SMA-DP-SGD, a spectral memory-aware extension of DP-SGD that reuses historical information in a privacy-compatible manner. The method constructs a fractional memory branch only from the private release history, namely previously privatized noisy gradient releases, rather than from raw historical gradients. Conditioned on this prior private history, the memory branch is fixed, so the update preserves a clean sensitivity structure while retaining an exact reduction to standard group-wise DP-SGD when the memory contribution is disabled.

SMA-DP-SGD combines fractional memory, WeightWatcher-inspired spectral tempering, private-history alignment, norm matching, and warm-up activation. In experiments, the group-wise formulation is instantiated layer-wise, allowing each trainable convolutional or linear layer to receive a spectral reliability signal. Across CIFAR-100, CIFAR-10, and MNIST, SMA-DP-SGD achieves competitive or superior accuracy compared with representative DP optimization baselines, with particularly strong behavior on more challenging image-classification settings. Ablations and diagnostics show that the fixed mixing coefficient controls the privacy-utility behavior, while the spectral-memory mechanism maintains a controlled effective memory depth and a small memory-branch contribution.

Several limitations remain. Because the memory branch is built from previous noisy private releases, it can inherit historical Gaussian noise along with useful optimization signal. The spectral reliability interval is also a tunable heuristic rather than a universal criterion for layer quality, and the spectral diagnostics introduce additional computational overhead. Moreover, full-step privacy guarantees require conservative joint accounting, while marginal privacy-cost curves should be interpreted only as diagnostics.

Future work should develop noise-aware private memory mechanisms that reduce the influence of inherited historical noise while remaining compatible with differential privacy. Other directions include adaptive spectral reliability ranges, cheaper spectral diagnostics, and extensions to federated learning, personalized private optimization, and private fine-tuning of larger models.

6 Broader Impact

SMA-DP-SGD aims to improve the utility of differentially private training by reusing historical information only through previously privatized releases. This may benefit privacy-sensitive applications such as healthcare, finance, mobile learning, and user-behavior modeling, where useful models must be trained under formal privacy constraints. However, improved private optimization does not remove the need for careful privacy accounting, transparent reporting of privacy budgets, and rigorous implementation. In particular, marginal privacy-cost diagnostics should not be interpreted as full-model privacy guarantees. The method also introduces additional computational overhead through spectral diagnostics and memory management. Responsible deployment should therefore combine SMA-DP-SGD with reproducible evaluation, conservative privacy analysis, and domain-specific risk assessment.

References

- Martin Abadi, Andy Chu, Ian Goodfellow, H. Brendan McMahan, Ilya Mironov, Kunal Talwar, and Li Zhang. Deep learning with differential privacy. In *Proceedings of the 2016 ACM SIGSAC Conference on Computer and Communications Security*, pages 308–318. ACM, 2016. doi: 10.1145/2976749.2978318.
- Galen Andrew, Om Thakkar, H. Brendan McMahan, and Swaroop Ramaswamy. Differentially private learning with adaptive clipping. In *Advances in Neural Information Processing Systems*, volume 34, pages 17455–17466, 2021.
- Peter L. Bartlett, Dylan J. Foster, and Matus J. Telgarsky. Spectrally-normalized margin bounds for neural networks. In *Advances in Neural Information Processing Systems*, volume 30, 2017.
- Raef Bassily, Adam Smith, and Abhradeep Thakurta. Private empirical risk minimization: Efficient algorithms and tight error bounds. In *Proceedings of the 2014 IEEE 55th Annual Symposium on Foundations of Computer Science*, pages 464–473. IEEE, 2014. doi: 10.1109/FOCS.2014.56.
- Zhiqi Bu, Jinshuo Dong, Qi Long, and Weijie J. Su. Deep learning with gaussian differential privacy. *Harvard Data Science Review*, 2020(23), 2020. doi: 10.1162/99608f92.cfc5dd25.
- Soham De, Leonard Berrada, Jamie Hayes, Samuel L. Smith, and Borja Balle. Unlocking high-accuracy differentially private image classification through scale. *arXiv preprint arXiv:2204.13650*, 2022.
- Kai Diethelm. *The Analysis of Fractional Differential Equations: An Application-Oriented Exposition Using Differential Operators of Caputo Type*, volume 2004 of *Lecture Notes in Mathematics*. Springer, 2010. doi: 10.1007/978-3-642-14574-2.
- John Duchi, Elad Hazan, and Yoram Singer. Adaptive subgradient methods for online learning and stochastic optimization. *Journal of Machine Learning Research*, 12:2121–2159, 2011.
- Cynthia Dwork and Aaron Roth. The algorithmic foundations of differential privacy. *Foundations and Trends in Theoretical Computer Science*, 9(3–4):211–407, 2014. doi: 10.1561/04000000042.
- Cynthia Dwork, Frank McSherry, Kobbi Nissim, and Adam Smith. Calibrating noise to sensitivity in private data analysis. In *Theory of Cryptography*, pages 265–284. Springer, 2006. doi: 10.1007/11681878_14.
- Pierre Foret, Ariel Kleiner, Hossein Mobahi, and Behnam Neyshabur. Sharpness-aware minimization for efficiently improving generalization. In *International Conference on Learning Representations*, 2021.
- Behrooz Ghorbani, Shankar Krishnan, and Ying Xiao. An investigation into neural net optimization via hessian eigenvalue density. In *Proceedings of the 36th International Conference on Machine Learning*, volume 97 of *Proceedings of Machine Learning Research*, pages 2232–2241. PMLR, 2019.

- Nitish Shirish Keskar, Dheevatsa Mudigere, Jorge Nocedal, Mikhail Smelyanskiy, and Ping Tak Peter Tang. On large-batch training for deep learning: Generalization gap and sharp minima. In *International Conference on Learning Representations*, 2017.
- Anatoly A. Kilbas, Hari M. Srivastava, and Juan J. Trujillo. *Theory and Applications of Fractional Differential Equations*, volume 204 of *North-Holland Mathematics Studies*. Elsevier, 2006. ISBN 9780444518323.
- Diederik P. Kingma and Jimmy Ba. Adam: A method for stochastic optimization. In *International Conference on Learning Representations*, 2015.
- Alex Krizhevsky. Learning multiple layers of features from tiny images. Technical report, University of Toronto, 2009.
- Yann LeCun, Léon Bottou, Yoshua Bengio, and Patrick Haffner. Gradient-based learning applied to document recognition. *Proceedings of the IEEE*, 86(11):2278–2324, 1998. doi: 10.1109/5.726791.
- Charles H. Martin and Michael W. Mahoney. Traditional and heavy-tailed self regularization in neural network models. In *Proceedings of the 36th International Conference on Machine Learning*, volume 97 of *Proceedings of Machine Learning Research*, pages 4284–4293. PMLR, 2019.
- Charles H. Martin and Michael W. Mahoney. Implicit self-regularization in deep neural networks. *Journal of Machine Learning Research*, 22(165):1–73, 2021.
- Charles H. Martin, Tongsu Peng, and Michael W. Mahoney. Predicting trends in the quality of state-of-the-art neural networks without access to training or testing data. *Nature Communications*, 12(1):4122, 2021. doi: 10.1038/s41467-021-24025-8.
- H. Brendan McMahan, Daniel Ramage, Kunal Talwar, and Li Zhang. Learning differentially private recurrent language models. In *International Conference on Learning Representations*, 2018.
- Mark M. Meerschaert and Alla Sikorskii. *Stochastic Models for Fractional Calculus*, volume 43 of *De Gruyter Studies in Mathematics*. De Gruyter, 2012. doi: 10.1515/9783110258165.
- Ilya Mironov. Rényi differential privacy. In *2017 IEEE 30th Computer Security Foundations Symposium*, pages 263–275. IEEE, 2017. doi: 10.1109/CSF.2017.11.
- Yurii E. Nesterov. A method for solving the convex programming problem with convergence rate $O(1/k^2)$. In *Doklady Akademii Nauk SSSR*, volume 269, pages 543–547, 1983.
- Behnam Neyshabur, Srinadh Bhojanapalli, David McAllester, and Nati Srebro. Exploring generalization in deep learning. In *Advances in Neural Information Processing Systems*, volume 30, 2017.
- Nicolas Papernot, Shuang Song, Ilya Mironov, Ananth Raghunathan, Kunal Talwar, and Úlfar Erlingsson. Scalable private learning with PATE. In *International Conference on Learning Representations*, 2018.
- Mohammad Partohaghighi, Roummel Marcia, Bruce J. West, and YangQuan Chen. When gradient clipping becomes a control mechanism for differential privacy in deep learning. *arXiv preprint arXiv:2602.10584*, 2026a. doi: 10.48550/arXiv.2602.10584.
- Mohammad Partohaghighi, Roummel Marcia, Bruce J. West, and YangQuan Chen. Statistical roughness-informed machine unlearning. *arXiv preprint arXiv:2602.09304*, 2026b. doi: 10.48550/arXiv.2602.09304.
- Mohammad Partohaghighi, Roummel Marcia, Bruce J. West, and Yangquan Chen. Roughness-informed differential privacy. *Expert Systems with Applications*, 313:131501, 2026c. doi: 10.1016/j.eswa.2026.131501.
- Jeffrey Pennington and Pratik Worah. Nonlinear random matrix theory for deep learning. In *Advances in Neural Information Processing Systems*, volume 30, 2017.

- Igor Podlubny. *Fractional Differential Equations: An Introduction to Fractional Derivatives, Fractional Differential Equations, to Methods of Their Solution and Some of Their Applications*, volume 198 of *Mathematics in Science and Engineering*. Academic Press, 1999. ISBN 9780125588409.
- Boris T. Polyak. Some methods of speeding up the convergence of iteration methods. *USSR Computational Mathematics and Mathematical Physics*, 4(5):1–17, 1964. doi: 10.1016/0041-5553(64)90137-5.
- Herbert Robbins and Sutton Monro. A stochastic approximation method. *The Annals of Mathematical Statistics*, 22(3):400–407, 1951. doi: 10.1214/aoms/1177729586.
- Florian Tramèr and Dan Boneh. Differentially private learning needs better features (or much more data). In *International Conference on Learning Representations*, 2021.
- Yu-Xiang Wang, Borja Balle, and Shiva Prasad Kasiviswanathan. Subsampled rényi differential privacy and analytical moments accountant. In *Proceedings of the Twenty-Second International Conference on Artificial Intelligence and Statistics*, volume 89 of *Proceedings of Machine Learning Research*, pages 1226–1235. PMLR, 2019.
- Bruce J. West. Colloquium: Fractional calculus view of complexity: A tutorial. *Reviews of Modern Physics*, 86(4):1169–1185, 2014. doi: 10.1103/RevModPhys.86.1169.

Appendix Overview

This appendix provides supplementary experimental details, additional empirical results, diagnostic analyses, runtime comparisons, and the full theoretical analysis supporting the main paper. To improve readability and navigation, the supplementary material is organized into two main parts. Appendix A provides additional experiments and reproducibility details, while Appendix B presents the theoretical analysis and interpretation of SMA-DP-SGD.

Appendix A: Additional Experiments and Reproducibility Details. This part complements the main experimental section. It includes the full experimental setup and reproducibility information, final-accuracy statistics on CIFAR-10, the diagnostic effect of the fixed mixing parameter on marginal privacy cost, effective fractional-memory diagnostics, and runtime comparisons. It also clarifies the layer-wise experimental instantiation of the group-wise formulation, the use of a shared fractional order α , a shared memory window K , and the reporting protocol for repeated runs and confidence intervals.

Appendix B: Theoretical Analysis and Interpretation of SMA-DP-SGD. This part analyzes SMA-DP-SGD from the perspective of recursive-query sensitivity, conservative joint Rényi differential privacy accounting, adaptive composition, mechanism-level interpretation, signal–memory–noise decomposition, and limiting regimes. It distinguishes the marginal group-wise noise-to-sensitivity diagnostic from the formal full-step joint accountant and establishes the exact reduction to group-wise DP-SGD when the memory contribution is disabled.

Navigation Guide. For convenience, the appendix is organized as follows:

- Appendix A: Additional experiments and reproducibility details.
- Appendix A.1: Experimental setup, baselines, parameter grouping, and reproducibility protocol.
- Appendix A.4: Final accuracy comparison on CIFAR-10 with mean, standard deviation, and 95% confidence intervals.
- Appendix A.5: Diagnostic effect of the fixed mixing parameter on marginal privacy cost.
- Appendix A.6: Diagnostic analysis of effective fractional memory depth and memory-branch ratio.
- Appendix A.7: Runtime comparison and computational overhead on CIFAR-10.
- Appendix B: Theoretical analysis and interpretation of SMA-DP-SGD.
- Appendix B.1: Standing assumptions and notation.
- Appendix B.3: Private-history-conditioned recursive-query sensitivity.
- Appendix B.4: Distinction between marginal group-wise diagnostics and full joint privacy accounting.
- Appendix B.5: Conservative joint per-step RDP accounting.
- Appendix B.6: Adaptive composition over training.
- Appendix B.8: Signal–memory–noise decomposition.
- Appendix B.9: Interpretation of spectral tempering and private-history gating.
- Appendix B.10: Special cases and limiting regimes.

Table 1: Summary of the main experimental configuration. Hyperparameters that vary across ablations are reported in the corresponding experiment-specific rows.

Quantity	Value / Description
Datasets	CIFAR-100, CIFAR-10, MNIST
Baselines	DP-SGD, DP-Adam, DP-AdamW, DP-IS, DP-SAM, DP-SAT, DP-Adam-AC
Parameter grouping	Layer-wise; each trainable convolutional or linear layer is one group
Spectral-dynamics model	ResNet-18 on CIFAR-10
Spectral interval	$I_\rho = [2, 6]$, unless otherwise stated
Mixing coefficient	Fixed β ; ablation uses $\{1.00, 0.90, 0.70, 0.50\}$
Final-accuracy setting	$\beta = 0.95, \alpha = 0.70, K = 4$
Spectral-interval diagnostic	Candidate intervals $[1, 3], [2, 4], [2, 6], [3, 5], [4, 6], [5, 7]$
Runtime setting	$\beta = 0.55, \alpha = 0.90, K = 8$
Repeated runs	Three independent runs for final-accuracy statistics
Statistical reporting	Mean, sample standard deviation, and two-sided 95% Student- t CI
Privacy-cost curves	Marginal group-wise diagnostic using σ/β
Formal privacy guarantee	Conservative joint accountant in Appendix B
Code availability	Not released at submission time; available upon reasonable request after publication

A Additional Experiments and Reproducibility Details

A.1 Experimental Setup and Reproducibility

Datasets and tasks. We evaluate SMA-DP-SGD on three standard image-classification benchmarks: CIFAR-100, CIFAR-10, and MNIST. These datasets provide different levels of visual complexity and allow us to assess whether the proposed private-release-history memory mechanism remains effective across both simple and more challenging private learning settings.

Baselines. We compare SMA-DP-SGD against representative differentially private optimization baselines, including DP-SGD, DP-Adam, DP-AdamW, DP-IS, DP-SAM, DP-SAT, and DP-Adam-AC. All methods are evaluated under matched dataset, privacy, model, and training configurations whenever they appear in the same comparison.

Model and parameter grouping. The methodology is formulated for generic parameter groups g . In the experiments, we instantiate this group-wise formulation layer-wise: each trainable convolutional or linear layer is treated as one parameter group. Consequently, group-wise quantities such as $C^{(g)}, s_t^{(g)}, \rho_t^{(g)}, \lambda_t^{(g)}(I_\rho), \nu_{t-1}^{(g)}, \Gamma_t^{(g)}$, and $\Psi_t^{(g)}$ are computed per layer. For the CIFAR-10 spectral-dynamics study, we use a ResNet-18 model and aggregate layer-wise spectral quantities into stage-wise averages for visualization.

SMA-DP-SGD configuration. Unless otherwise stated, SMA-DP-SGD uses a fixed current-memory mixing coefficient β , a shared fractional order α , and a shared memory window K across all parameter groups. The memory branch is constructed only from the private release history, i.e., previously privatized noisy releases, and is controlled by spectral tempering, private-history alignment, norm matching, and warm-up activation. The case $\beta = 1$ corresponds to the exact DP-SGD limiting case with no memory contribution.

Repeated runs and statistical reporting. For final-accuracy comparisons on CIFAR-10, each method is evaluated over three independent runs. We report the mean final test accuracy, sample standard deviation, and two-sided 95% confidence interval computed using the Student- t interval.

Reproducibility and code availability. To support reproducibility, all compared methods use the same dataset split, model configuration, training horizon, sampling protocol, clipping setup, and privacy noise configuration within each experiment. The main experimental configuration is summarized in Table 1. The source code is not released at submission time. If the paper is published, we plan to provide the implementation and scripts upon reasonable request to support reproduction of the reported results.

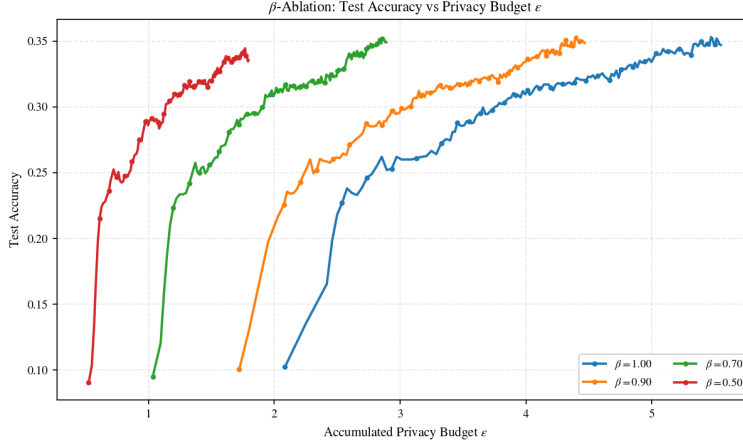


Figure 3: Ablation study of the fixed current-memory mixing parameter β for SMA-DP-SGD on CIFAR-10. The figure reports test accuracy versus accumulated privacy budget for $\beta \in \{1.00, 0.90, 0.70, 0.50\}$.

A.2 Ablation Study on the Fixed Mixing Parameter on CIFAR-10

To analyze the role of the fixed current-memory mixing parameter β , we evaluate the privacy–utility behavior of SMA-DP-SGD on CIFAR-10 under different fixed values of β . We compare $\beta \in \{1.00, 0.90, 0.70, 0.50\}$, where $\beta = 1.00$ corresponds to the standard DP-SGD limiting case, while smaller values introduce stronger private-release-history fractional memory effects into the optimization dynamics. The resulting test accuracy as a function of accumulated privacy budget is shown in Fig. 3.

As shown in Fig. 3, the choice of β substantially affects the privacy–utility trajectory. The limiting case $\beta = 1.00$ requires a larger privacy budget to reach high test accuracy. In contrast, smaller values of β , especially $\beta = 0.70$ and $\beta = 0.50$, reach comparable or higher accuracy using a smaller privacy budget in this diagnostic. The curve for $\beta = 0.90$ provides an intermediate trade-off between the standard DP-SGD update and stronger memory-based regimes. These results suggest that private-release-history fractional memory can improve optimization efficiency when the memory contribution remains controlled.

A.3 Stage-Wise Spectral Dynamics and Tempering on CIFAR-10

To further analyze SMA-DP-SGD, we study the evolution of the WeightWatcher-style spectral exponent and its induced tempering coefficient across different stages of the CIFAR-10 ResNet-18 model. Since ResNet-18 contains many convolutional and linear parameter groups, directly plotting all group-wise spectral trajectories would be visually cluttered. Therefore, we aggregate layer-wise quantities into stage-wise averages.

Let $\mathcal{G}_{\text{stage}}$ denote the set of convolutional or linear parameter groups belonging to a given ResNet stage, such as the stem, stage1, stage2, stage3, stage4, or the final classifier. For each epoch t , we define the stage-wise spectral exponent as

$$\bar{\rho}_t^{(\text{stage})} = \frac{1}{|\mathcal{G}_{\text{stage}}|} \sum_{g \in \mathcal{G}_{\text{stage}}} \rho_t^{(g)}. \quad (1)$$

Similarly, we define the stage-wise tempering coefficient as

$$\bar{\lambda}_t^{(\text{stage})} = \frac{1}{|\mathcal{G}_{\text{stage}}|} \sum_{g \in \mathcal{G}_{\text{stage}}} \lambda_t^{(g)}(I_\rho). \quad (2)$$

These diagnostics summarize the spectral evolution and induced memory-decay policy of each major ResNet component while preserving the layer-aware nature of SMA-DP-SGD.

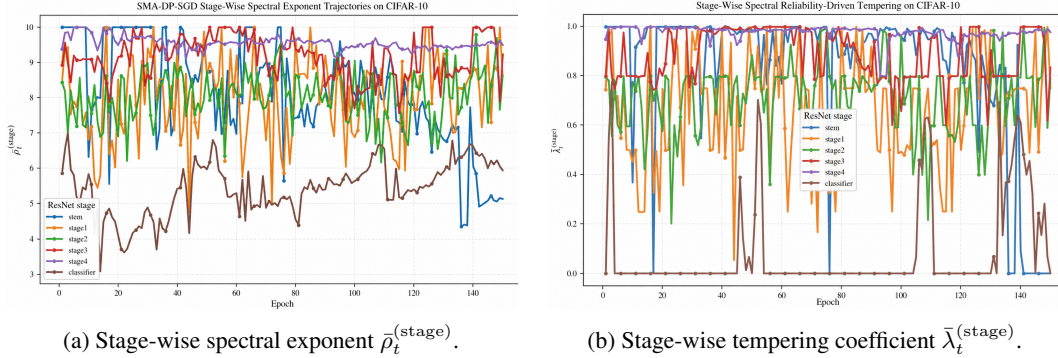


Figure 4: Stage-wise spectral dynamics and reliability-driven tempering of SMA-DP-SGD on CIFAR-10. Panel a reports the stage-wise average spectral exponent over convolutional or linear parameter groups within each ResNet-18 component. Panel b reports the corresponding stage-wise average tempering coefficient.

The favorable spectral-reliability interval $I_\rho = [2, 6]$ is used as a heuristic for controlling the memory horizon. Groups closer to this interval receive weaker tempering and retain longer private-release-history memory, whereas groups farther from the interval receive stronger tempering and forget older releases more aggressively.

Figure 4 reports both the stage-wise spectral exponent trajectories and the induced stage-wise tempering coefficients. The results show that different ResNet components occupy different spectral regimes during private optimization. The tempering plot illustrates how these spectral states are translated into stage-dependent memory-decay coefficients. This supports the use of a layer-wise spectral memory policy rather than a single uniform memory horizon for all parts of the network.

The stage-wise variation in $\bar{\rho}_t^{(\text{stage})}$ and $\bar{\lambda}_t^{(\text{stage})}$ does not imply that the mixing coefficient β is adaptive. In our formulation, β is fixed and globally controls the interpolation between the current clipped gradient sum and the private-release-history memory branch. The adaptive quantities are the spectral exponent, spectral deviation, tempering coefficient, and effective memory depth.

A.4 Final Accuracy Comparison on CIFAR-10

To evaluate the stability and final predictive performance of SMA-DP-SGD, we compare its final test accuracy against several differentially private optimizer baselines on CIFAR-10. Each method is evaluated over three independent runs, and we report the mean final test accuracy, sample standard deviation, and a two-sided 95% confidence interval.

As shown in Table 2, SMA-DP-SGD achieves the highest final test accuracy among all compared methods. The proposed method obtains 0.3463 ± 0.0003 , with a narrow 95% confidence interval of $[0.3456, 0.3471]$. This indicates not only a higher mean final accuracy, but also substantially lower run-to-run variability compared with several DP optimizer baselines.

The improvement is consistent with the intended role of the spectral memory-aware mechanism. In this experiment, $\beta = 0.95$, $\alpha = 0.70$, and $K = 4$, meaning that the method remains close to the current private gradient update while allowing a controlled fractional-memory contribution.

A.5 Diagnostic Effect of the Mixing Parameter on Marginal Privacy Cost

We further study the effect of the fixed current-memory mixing parameter β on the marginal privacy-cost trajectory of SMA-DP-SGD on CIFAR-10. This diagnostic uses the marginal group-wise ratio σ/β to visualize how β affects the current-query noise-to-sensitivity ratio for an individual group. It should not be interpreted as the formal full-model privacy guarantee; the formal guarantee follows the conservative joint accountant in Appendix B.

Figure 5 shows the resulting marginal accumulated privacy-cost trajectory as a function of epoch for different fixed values of β . The results follow the expected monotonic pattern: $\beta = 1.00$,

Table 2: Final CIFAR-10 test accuracy over three independent runs. We report mean, sample standard deviation, and two-sided 95% confidence intervals.

Algorithm	Mean \pm std	95% CI
DP-SGD	0.3382 \pm 0.0031	[0.3306, 0.3458]
DP-Adam	0.3295 \pm 0.0095	[0.3058, 0.3532]
DP-AdamW	0.3203 \pm 0.0070	[0.3029, 0.3378]
DP-IS	0.3278 \pm 0.0023	[0.3222, 0.3334]
DP-SAM	0.3215 \pm 0.0105	[0.2954, 0.3476]
DP-SAT	0.3215 \pm 0.0105	[0.2954, 0.3476]
DP-Adam-AC	0.3073 \pm 0.0139	[0.2728, 0.3419]
SMA-DP-SGD	0.3463 \pm 0.0003	[0.3456, 0.3471]

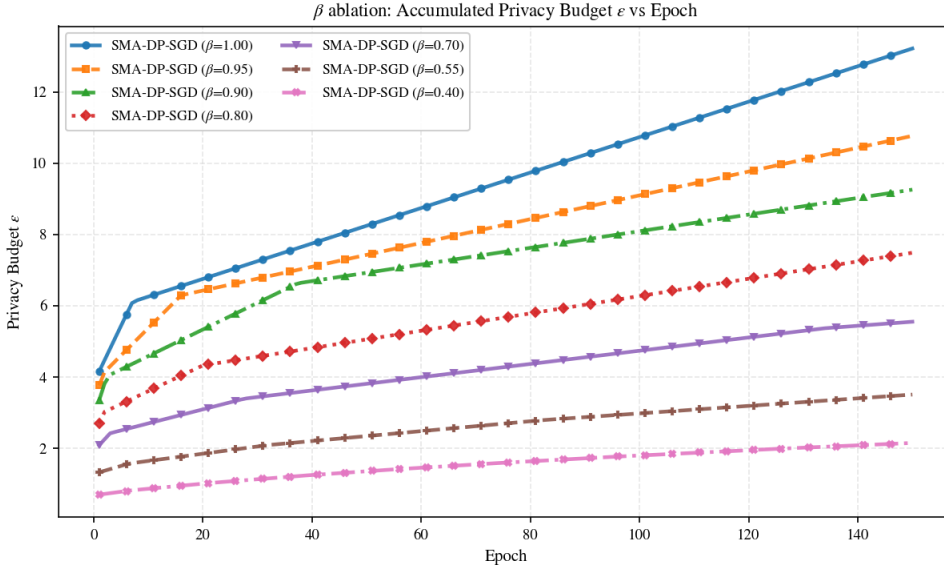


Figure 5: Diagnostic effect of the fixed current-memory mixing parameter β on the marginal group-wise accumulated privacy cost of SMA-DP-SGD on CIFAR-10. The curves use the marginal effective ratio σ/β . The formal full-step privacy guarantee follows the conservative joint accountant in Appendix B.

corresponding to the DP-SGD special case with no memory contribution, has the largest marginal privacy cost. As β decreases, the marginal privacy cost becomes progressively smaller.

This reduction is not a free privacy improvement: smaller β also attenuates the direct current-gradient signal and increases reliance on historical private releases. Therefore, β should be selected by considering both utility and privacy.

A.6 Spectral Interval Sensitivity of Effective Fractional Memory

To assess the sensitivity of the memory mechanism to the spectral reliability interval, we evaluate SMA-DP-SGD under different choices of I_ρ . The interval I_ρ determines which spectral exponent values are treated as reliable by the memory controller. Intervals that include the observed layer-wise spectral exponents more often tend to produce weaker tempering and therefore longer effective memory, whereas intervals farther from the observed spectral regime induce stronger tempering and shorter memory depth.

As reported in Table 3, the effective memory depth varies noticeably across spectral intervals. The interval $[2, 6]$ yields the largest mean effective memory depth, followed closely by $[2, 4]$, indicating that these intervals allow the private-release-history memory branch to retain a longer temporal horizon. In contrast, intervals such as $[4, 6]$ and $[5, 7]$ produce shorter effective memory depths, suggesting stronger spectral tempering and faster decay of older private releases. The mean memory

Table 3: Sensitivity of SMA-DP-SGD to the spectral reliability interval I_ρ on CIFAR-10. The table reports the mean effective memory depth and the mean memory-branch ratio for different choices of I_ρ .

Spectral interval I_ρ	Mean D_{eff}	Mean memory ratio
[1, 3]	2.7636	0.0065
[2, 4]	3.0902	0.0136
[2, 6]	3.2079	0.0133
[3, 5]	2.7487	0.0113
[4, 6]	1.9857	0.0072
[5, 7]	1.6749	0.0027

Table 4: Relative runtime comparison on CIFAR-10. Runtime is measured in seconds and normalized by DP-SGD.

Algorithm	Mean (s)	Mean \pm std (s)	Rel. runtime
DP-SGD	92.66	92.66 \pm 0.00	1.00 \times
DP-Adam	92.75	92.75 \pm 0.00	1.00 \times
DP-AdamW	91.83	91.83 \pm 0.00	0.99 \times
DP-IS	98.84	98.84 \pm 0.00	1.07 \times
DP-SAM	172.25	172.25 \pm 0.00	1.86 \times
DP-SAT	167.63	167.63 \pm 0.00	1.81 \times
SMA-DP-SGD ($\beta = 0.55, \alpha = 0.90, K = 8$)	272.52	272.52 \pm 0.00	2.94 \times

ratio remains small for all intervals, indicating that the memory branch acts as a bounded correction rather than dominating the private update.

A.7 Runtime Comparison on CIFAR-10

To assess the computational overhead of SMA-DP-SGD, we compare the wall-clock runtime of the proposed method against differentially private optimizer baselines on CIFAR-10. Runtime is measured for the full training procedure under the same dataset size, model configuration, privacy parameters, and number of epochs.

As shown in Table 4, DP-SGD, DP-Adam, and DP-AdamW have nearly identical runtimes. DP-IS incurs a modest overhead of 1.07 \times , while DP-SAM and DP-SAT require approximately 1.86 \times and 1.81 \times the runtime of DP-SGD, respectively. SMA-DP-SGD has the largest runtime in this comparison, requiring 2.94 \times the runtime of DP-SGD. This overhead comes from the layer-wise spectral diagnostics, the maintenance of the private release history, and the computation of the tempered fractional memory branch for each parameter group.

B Theoretical Analysis and Interpretation of SMA-DP-SGD

This section analyzes SMA-DP-SGD from the perspectives of recursive-query sensitivity, conservative joint Rényi differential privacy (RDP) accounting, adaptive composition, mechanism-level interpretation, memory-noise decomposition, and limiting regimes. The analysis corresponds to the private-release-history version of SMA-DP-SGD.

For each parameter group g , the recursive query is

$$r_t^{(g)}(D; m_t, \mathcal{H}_t) = \beta s_t^{(g)}(D; m_t) + b_t^{(g)}(\mathcal{H}_t), \quad (3)$$

where $s_t^{(g)}(D; m_t)$ is the current group-wise clipped subsampled sum and

$$b_t^{(g)}(\mathcal{H}_t) = (1 - \beta)\omega_t \Gamma_t^{(g)} \Psi_t^{(g)} \nu_{t-1}^{(g)} \quad (4)$$

is the memory branch computed from the prior private release history.

The global private release history is

$$\mathcal{H}_t = (\mathcal{H}_t^{(1)}, \dots, \mathcal{H}_t^{(G)}), \quad \mathcal{H}_t^{(g)} = (\tilde{s}_0^{(g)}, \dots, \tilde{s}_{t-1}^{(g)}). \quad (5)$$

This private release history is the private transcript in the adaptive composition view. We condition on the global history rather than only the group-wise history because the current model state θ_t , spectral diagnostics, private EMA trends, and group-wise gradients may depend on all previous group-wise private releases. The central private-release-history property is that

$$\nu_{t-1}^{(g)}, \quad \Gamma_t^{(g)}, \quad \Psi_t^{(g)}, \quad \lambda_t^{(g)}(I_\rho), \quad \mu_{t-1}^{(g)}$$

are deterministic functions of \mathcal{H}_t , the model state induced by previous private releases, and public hyperparameters. They do not depend on the current clipped sum $s_t^{(g)}$. Consequently, once \mathcal{H}_t is fixed, the entire memory branch $b_t^{(g)}(\mathcal{H}_t)$ is fixed, and the only newly data-dependent component of $r_t^{(g)}$ is the scaled clipped sum $\beta s_t^{(g)}$.

B.1 Standing Assumptions and Notation

Add/remove adjacency. We use add/remove adjacency. Two datasets D and D' are adjacent, denoted $D \sim D'$, if one can be obtained from the other by adding or removing one example.

Poisson subsampling. At private step t , a Poisson mask $m_t = (m_{t,1}, \dots, m_{t,N})$ is drawn with

$$m_{t,i} \sim \text{Bernoulli}(q_t)$$

independently across examples. The sampled set is

$$S_t = \{i : m_{t,i} = 1\}.$$

The same sampling event is used for the joint vector release across all parameter groups at step t .

Group-wise clipping. For each group g , the per-example gradient is clipped as

$$\bar{g}_t^{(g)}(x_i) = \frac{g_t^{(g)}(x_i)}{\max\left(1, \frac{\|g_t^{(g)}(x_i)\|_2}{C^{(g)}}\right)}, \quad (6)$$

so that

$$\|\bar{g}_t^{(g)}(x_i)\|_2 \leq C^{(g)}. \quad (7)$$

The group-wise clipped subsampled sum is

$$s_t^{(g)}(D; m_t) = \sum_{i=1}^N m_{t,i} \bar{g}_t^{(g)}(x_i). \quad (8)$$

Private-release-history memory branch. For each group g , the memory branch is

$$b_t^{(g)}(\mathcal{H}_t) = (1 - \beta)\omega_t \Gamma_t^{(g)} \Psi_t^{(g)} \nu_{t-1}^{(g)}.$$

All quantities inside this branch are deterministic functions of the global prior private release history \mathcal{H}_t , the current model state induced by previous private releases, and public hyperparameters. In particular, the private-history alignment gate $\Gamma_t^{(g)}$ and norm scale $\Psi_t^{(g)}$ do not depend on the current clipped sum $s_t^{(g)}$.

Shared and group-wise memory parameters. The fractional order $\alpha \in (0, 1]$ and memory window K are shared across parameter groups. The number of available lags at step t is therefore

$$M_t = \min(K - 1, t).$$

Group-wise adaptivity of the memory kernel enters through the spectral tempering coefficient $\lambda_t^{(g)}(I_\rho)$, which depends on the group-wise spectral exponent $\rho_t^{(g)}$.

Gaussian perturbation. For each group g , the group-wise release is

$$\tilde{s}_t^{(g)} = r_t^{(g)} + Z_t^{(g)}, \quad Z_t^{(g)} \sim \mathcal{N}\left(0, \sigma_{t,g}^2 (C^{(g)})^2 I_g\right), \quad (9)$$

where I_g is the identity matrix with the dimension of group g . Noise is independent across groups conditional on the current step.

B.2 Fixed-Mask Group-Wise Clipped-Sum Sensitivity

We first recall the fixed-mask sensitivity of the group-wise clipped sum.

Lemma 1 (Fixed-mask sensitivity of the group-wise clipped sum). *Fix an iteration t , a group g , a model state θ_t , and a sampling mask m_t . Under add/remove adjacency,*

$$\Delta_s^{(g)}(m_t) := \sup_{D \sim D'} \left\| s_t^{(g)}(D; m_t) - s_t^{(g)}(D'; m_t) \right\|_2 \leq C^{(g)}. \quad (10)$$

Proof. Under add/remove adjacency, the datasets D and D' differ in at most one example. For a fixed sampling mask m_t , the two clipped sums can therefore differ in at most one clipped per-example contribution in group g . By Eq. (7), this contribution has norm at most $C^{(g)}$. Hence

$$\left\| s_t^{(g)}(D; m_t) - s_t^{(g)}(D'; m_t) \right\|_2 \leq C^{(g)}.$$

Taking the supremum over adjacent datasets gives the result. \square

The fixed-mask argument gives a conditional sensitivity bound. The randomness of Poisson subsampling, and the corresponding privacy amplification, are accounted for later through the subsampled Gaussian RDP bound.

B.3 Private-History-Conditioned Recursive-Query Sensitivity

The next result formalizes why the private-release-history construction yields a clean sensitivity bound.

Proposition 1 (Global private-history-conditioned memory branch). *Fix an iteration t , a group g , a realizable global prior private release history \mathcal{H}_t , and public hyperparameters. Then $b_t^{(g)}(\mathcal{H}_t)$ is fixed under this conditioning. Consequently, the only newly data-dependent term in*

$$r_t^{(g)}(D; m_t, \mathcal{H}_t) = \beta s_t^{(g)}(D; m_t) + b_t^{(g)}(\mathcal{H}_t)$$

is the scaled clipped sum $\beta s_t^{(g)}(D; m_t)$.

Proof. By the private-release-history design, the fractional memory state $\nu_{t-1}^{(g)}$, private EMA trend $\mu_{t-1}^{(g)}$, spectral tempering coefficient $\lambda_t^{(g)}(I_\rho)$, alignment gate $\Gamma_t^{(g)}$, and norm scale $\Psi_t^{(g)}$ are deterministic functions of the global prior private release history \mathcal{H}_t , the model state induced by previous private releases, and public hyperparameters. Therefore, once \mathcal{H}_t is fixed, all these quantities are fixed. Their product in Eq. (4) is also fixed. Hence the only newly data-dependent term in the recursive query is $\beta s_t^{(g)}(D; m_t)$. \square

Definition 1 (Private-history- and mask-conditioned group-wise recursive-query sensitivity). *For fixed \mathcal{H}_t and m_t , define*

$$\Delta_r^{(g)}(m_t, \mathcal{H}_t) = \sup_{D \sim D'} \left\| r_t^{(g)}(D; m_t, \mathcal{H}_t) - r_t^{(g)}(D'; m_t, \mathcal{H}_t) \right\|_2. \quad (11)$$

Theorem 1 (Conditional sensitivity of SMA-DP-SGD). *Fix an iteration t , a group g , a realizable global prior private release history \mathcal{H}_t , and a sampling mask m_t . Under add/remove adjacency,*

$$\Delta_r^{(g)}(m_t, \mathcal{H}_t) \leq \beta C^{(g)}. \quad (12)$$

Proof. For adjacent datasets $D \sim D'$, using Eq. (3),

$$\begin{aligned}
& r_t^{(g)}(D; m_t, \mathcal{H}_t) - r_t^{(g)}(D'; m_t, \mathcal{H}_t) \\
&= \left[\beta s_t^{(g)}(D; m_t) + b_t^{(g)}(\mathcal{H}_t) \right] - \left[\beta s_t^{(g)}(D'; m_t) + b_t^{(g)}(\mathcal{H}_t) \right] \\
&= \beta \left[s_t^{(g)}(D; m_t) - s_t^{(g)}(D'; m_t) \right] + \underbrace{b_t^{(g)}(\mathcal{H}_t) - b_t^{(g)}(\mathcal{H}_t)}_{=0} \\
&= \beta \left[s_t^{(g)}(D; m_t) - s_t^{(g)}(D'; m_t) \right].
\end{aligned}$$

Taking norms and applying Lemma 1 gives

$$\left\| r_t^{(g)}(D; m_t, \mathcal{H}_t) - r_t^{(g)}(D'; m_t, \mathcal{H}_t) \right\|_2 \leq \beta C^{(g)}.$$

Taking the supremum over adjacent datasets proves the claim. \square

Remark 1 (Why current-gradient-dependent gates are excluded). *The cancellation in Theorem 1 depends critically on the memory branch being computed from the prior private release history. If $\Gamma_t^{(g)}$ or $\Psi_t^{(g)}$ depended on the current clipped sum $s_t^{(g)}$, then the memory branch would generally differ between adjacent datasets, and the bound $\Delta_r^{(g)} \leq \beta C^{(g)}$ would not follow from the above argument.*

B.4 Marginal Group-Wise Ratio versus Joint Full-Step Accountant

For a single group g viewed in isolation, the conditional sensitivity from Theorem 1 is $\beta C^{(g)}$, while the Gaussian standard deviation is $\sigma_{t,g} C^{(g)}$. Thus, the marginal group-wise effective noise-to-sensitivity ratio is

$$\frac{\sigma_{t,g} C^{(g)}}{\beta C^{(g)}} = \frac{\sigma_{t,g}}{\beta}. \tag{13}$$

This ratio is useful for interpreting group-wise diagnostics and the role of β : decreasing β increases the marginal noise-to-sensitivity ratio for the current group-wise query.

However, the marginal ratio in Eq. (13) is not, by itself, a full-model privacy guarantee when all groups are released jointly. Because SMA-DP-SGD releases the vector of all group-wise noisy quantities under the same Poisson subsampling event, the formal full-step privacy guarantee uses the conservative joint accountant derived below. Therefore, empirical curves based on the σ/β ratio should be interpreted as marginal group-wise privacy-cost diagnostics unless $G = 1$ or an explicit composition over groups is performed.

B.5 Joint Per-Step RDP Accounting

The group-wise sensitivity bound is useful, but the full per-step mechanism releases all groups under the same Poisson subsampling event. Therefore, the main privacy statement is formulated for the joint vector release.

Define the joint recursive query and joint release as

$$r_t(D; m_t, \mathcal{H}_t) = \left(r_t^{(1)}(D; m_t, \mathcal{H}_t), \dots, r_t^{(G)}(D; m_t, \mathcal{H}_t) \right), \tag{14}$$

and

$$\tilde{s}_t = \left(\tilde{s}_t^{(1)}, \dots, \tilde{s}_t^{(G)} \right) = r_t(D; m_t, \mathcal{H}_t) + Z_t. \tag{15}$$

The noise vector Z_t has block-diagonal covariance

$$\Sigma_t = \text{diag} \left(\sigma_{t,1}^2 (C^{(1)})^2 I_1, \dots, \sigma_{t,G}^2 (C^{(G)})^2 I_G \right). \tag{16}$$

Definition 2 (Whitened joint sensitivity). *For fixed \mathcal{H}_t and m_t , define the whitened joint sensitivity*

$$\Delta_{\text{white},t} = \sup_{D \sim D'} \left\| \Sigma_t^{-1/2} [r_t(D; m_t, \mathcal{H}_t) - r_t(D'; m_t, \mathcal{H}_t)] \right\|_2. \tag{17}$$

Lemma 2 (Bound on the whitened joint sensitivity). *For fixed \mathcal{H}_t and m_t ,*

$$\Delta_{\text{white},t} \leq \beta \left(\sum_{g=1}^G \sigma_{t,g}^{-2} \right)^{1/2}. \quad (18)$$

Proof. For adjacent datasets $D \sim D'$, let

$$\delta_t^{(g)} = r_t^{(g)}(D; m_t, \mathcal{H}_t) - r_t^{(g)}(D'; m_t, \mathcal{H}_t).$$

By Theorem 1,

$$\left\| \delta_t^{(g)} \right\|_2 \leq \beta C^{(g)}.$$

The squared whitened norm of the joint difference is

$$\left\| \Sigma_t^{-1/2} [r_t(D; m_t, \mathcal{H}_t) - r_t(D'; m_t, \mathcal{H}_t)] \right\|_2^2 = \sum_{g=1}^G \frac{\left\| \delta_t^{(g)} \right\|_2^2}{\sigma_{t,g}^2 (C^{(g)})^2} \leq \sum_{g=1}^G \frac{\beta^2 (C^{(g)})^2}{\sigma_{t,g}^2 (C^{(g)})^2} = \beta^2 \sum_{g=1}^G \sigma_{t,g}^{-2}.$$

Taking square roots and then the supremum over adjacent datasets gives the claim. \square

Define the conservative effective joint noise-to-sensitivity ratio

$$\sigma_{\text{eff},t} = \frac{1}{\beta \left(\sum_{g=1}^G \sigma_{t,g}^{-2} \right)^{1/2}}. \quad (19)$$

If all groups use the same noise multiplier $\sigma_{t,g} = \sigma_t$, then

$$\sigma_{\text{eff},t} = \frac{\sigma_t}{\beta \sqrt{G}}. \quad (20)$$

Remark 2 (Conservativeness of the joint bound). *The bound in Lemma 2 is a valid upper bound obtained from the individual group-wise sensitivity bounds. It may be conservative if the true concatenated contribution of a single example across groups is smaller than the worst-case combination of all group-wise clipping bounds. We do not claim that this joint accounting is tight. In particular, the joint effective ratio in Eq. (19) can be substantially smaller than the marginal group-wise ratio $\sigma_{t,g}/\beta$.*

Let

$$\varepsilon_{\text{SGM}}(\lambda_R; q, \sigma)$$

denote any valid RDP upper bound at order $\lambda_R > 1$ for the Poisson-subsampled Gaussian mechanism with subsampling probability q and noise-to-sensitivity ratio σ .

Theorem 2 (Joint per-step RDP guarantee). *Fix an iteration t and a realizable global prior private release history \mathcal{H}_t . The joint release*

$$\tilde{s}_t = r_t(D; m_t, \mathcal{H}_t) + Z_t, \quad Z_t \sim \mathcal{N}(0, \Sigma_t),$$

with Poisson subsampling probability q_t , satisfies

$$(\lambda_R, \varepsilon_{\text{SGM}}(\lambda_R; q_t, \sigma_{\text{eff},t}))\text{-RDP} \quad (21)$$

for every $\lambda_R > 1$.

Proof. Conditioned on the global prior private release history \mathcal{H}_t , all memory branches are fixed. The current data access at step t occurs through the same Poisson subsampling event m_t for the joint vector release.

By Lemma 2, the joint recursive query has whitened sensitivity at most

$$\Delta_{\text{white},t} \leq \beta \left(\sum_{g=1}^G \sigma_{t,g}^{-2} \right)^{1/2}.$$

Whitening by $\Sigma_t^{-1/2}$ transforms the anisotropic Gaussian release into an isotropic Gaussian mechanism with identity covariance and normalized sensitivity bounded by $\Delta_{\text{white},t}$. Hence the effective noise-to-sensitivity ratio is at least

$$\frac{1}{\Delta_{\text{white},t}} \geq \frac{1}{\beta \left(\sum_{g=1}^G \sigma_{t,g}^{-2} \right)^{1/2}} = \sigma_{\text{eff},t}.$$

Therefore, any valid RDP upper bound for the Poisson-subsampled Gaussian mechanism applies with effective ratio $\sigma_{\text{eff},t}$, yielding Eq. (21). \square

B.6 Adaptive Composition over Training

SMA-DP-SGD is adaptive because later model states and memory branches depend on previous private releases. RDP adaptive composition applies because each step conditions on the prior private release history and then releases a valid private joint mechanism.

Theorem 3 (Adaptive composition for SMA-DP-SGD). *Suppose SMA-DP-SGD is run for T private steps. For every $\lambda_R > 1$, the full release history satisfies*

$$(\lambda_R, \varepsilon_{\text{tot}}(\lambda_R))\text{-RDP}, \quad (22)$$

where

$$\varepsilon_{\text{tot}}(\lambda_R) = \sum_{t=0}^{T-1} \varepsilon_{\text{SGM}}(\lambda_R; q_t, \sigma_{\text{eff},t}). \quad (23)$$

Consequently, for any $\delta \in (0, 1)$, SMA-DP-SGD satisfies $(\varepsilon_\delta, \delta)$ -DP with

$$\varepsilon_\delta = \inf_{\lambda_R > 1} \left\{ \varepsilon_{\text{tot}}(\lambda_R) + \frac{\log(1/\delta)}{\lambda_R - 1} \right\}. \quad (24)$$

Proof. By Theorem 2, the joint release at step t satisfies

$$(\lambda_R, \varepsilon_{\text{SGM}}(\lambda_R; q_t, \sigma_{\text{eff},t}))\text{-RDP}.$$

Although the algorithm is adaptive, this adaptivity is through prior private releases. Adaptive composition of RDP permits summing the per-step RDP costs, which gives Eq. (23). The standard conversion from RDP to (ε, δ) -DP yields Eq. (24). \square

B.7 Mechanism-Level Interpretation

SMA-DP-SGD uses prior private releases to construct its memory branch. This memory construction is post-processing of the prior private release history. However, the current step is not merely post-processing of a standard DP-SGD release. Instead, SMA-DP-SGD forms a new history-dependent recursive query and then privatizes that query with fresh Gaussian noise.

Definition 3 (Standard and SMA-DP-SGD group-wise queries). *At step t , define the standard group-wise DP-SGD clipped-sum query as*

$$q_t^{\text{DP-SGD},(g)}(D; m_t) = s_t^{(g)}(D; m_t), \quad (25)$$

and the SMA-DP-SGD recursive query as

$$q_t^{\text{SMA},(g)}(D; m_t, \mathcal{H}_t) = \beta s_t^{(g)}(D; m_t) + b_t^{(g)}(\mathcal{H}_t). \quad (26)$$

Proposition 2 (Mechanism-level modification). *Suppose $0 < \beta < 1$ and $b_t^{(g)}(\mathcal{H}_t) \neq 0$. Then the SMA-DP-SGD query differs structurally from the standard group-wise DP-SGD clipped-sum query. In particular, SMA-DP-SGD forms a history-dependent recursive query before adding fresh Gaussian noise and is therefore not merely post-processing of a standard DP-SGD private release.*

Proof. The standard group-wise DP-SGD query is

$$q_t^{\text{DP-SGD},(g)}(D; m_t) = s_t^{(g)}(D; m_t).$$

The SMA-DP-SGD query is

$$q_t^{\text{SMA},(g)}(D; m_t, \mathcal{H}_t) = \beta s_t^{(g)}(D; m_t) + b_t^{(g)}(\mathcal{H}_t).$$

When $0 < \beta < 1$ and $b_t^{(g)}(\mathcal{H}_t) \neq 0$, this query contains a nonzero history-dependent memory branch and a scaled current clipped sum. Therefore, the query object is structurally different from the standard DP-SGD clipped-sum query.

Moreover, SMA-DP-SGD releases

$$\tilde{s}_t^{(g)} = q_t^{\text{SMA},(g)}(D; m_t, \mathcal{H}_t) + Z_t^{(g)},$$

so fresh Gaussian noise is applied after the recursive query is formed. Thus, privacy follows from fresh Gaussian perturbation of the history-dependent query together with the conditional sensitivity bound, not merely from post-processing a standard DP-SGD release. \square

B.8 Signal–Memory–Noise Decomposition

The private-release-history memory branch reuses previous noisy private releases. This can carry useful optimization signal, but it also carries inherited Gaussian noise.

In this analysis, the fractional order α and memory window K are shared across parameter groups. Group-wise adaptivity of the memory kernel enters through $\lambda_t^{(g)}(I_\rho)$, which depends on the group-wise spectral exponent $\rho_t^{(g)}$. Let

$$M_t = \min(K - 1, t).$$

For $M_t \geq 1$, the fractional memory state is

$$\nu_{t-1}^{(g)} = \sum_{j=1}^{M_t} \hat{a}_{t,j}^{(g)} \tilde{s}_{t-j}^{(g)}. \quad (27)$$

Each previous private release satisfies

$$\tilde{s}_{t-j}^{(g)} = r_{t-j}^{(g)} + Z_{t-j}^{(g)}.$$

Lemma 3 (Algebraic signal–memory–noise decomposition). *For $M_t \geq 1$, the memory state admits the algebraic decomposition*

$$\nu_{t-1}^{(g)} = \nu_{t-1}^{\text{rec},(g)} + \nu_{t-1}^{\text{noise},(g)}, \quad (28)$$

where

$$\nu_{t-1}^{\text{rec},(g)} = \sum_{j=1}^{M_t} \hat{a}_{t,j}^{(g)} r_{t-j}^{(g)} \quad (29)$$

and

$$\nu_{t-1}^{\text{noise},(g)} = \sum_{j=1}^{M_t} \hat{a}_{t,j}^{(g)} Z_{t-j}^{(g)}. \quad (30)$$

Consequently,

$$\begin{aligned} r_t^{(g)} &= \beta s_t^{(g)} + (1 - \beta) \omega_t \Gamma_t^{(g)} \Psi_t^{(g)} \nu_{t-1}^{\text{rec},(g)} \\ &\quad + (1 - \beta) \omega_t \Gamma_t^{(g)} \Psi_t^{(g)} \nu_{t-1}^{\text{noise},(g)}. \end{aligned} \quad (31)$$

Proof. Substituting

$$\tilde{s}_{t-j}^{(g)} = r_{t-j}^{(g)} + Z_{t-j}^{(g)}$$

into Eq. (27) gives

$$\begin{aligned} \nu_{t-1}^{(g)} &= \sum_{j=1}^{M_t} \hat{a}_{t,j}^{(g)} \left(r_{t-j}^{(g)} + Z_{t-j}^{(g)} \right) \\ &= \sum_{j=1}^{M_t} \hat{a}_{t,j}^{(g)} r_{t-j}^{(g)} + \sum_{j=1}^{M_t} \hat{a}_{t,j}^{(g)} Z_{t-j}^{(g)}. \end{aligned}$$

This proves Eq. (28). Substituting this decomposition into the recursive query gives Eq. (31). \square

Remark 3 (Algebraic, not independence-based). *The decomposition in Lemma 3 is algebraic. The weights $\hat{a}_{t,j}^{(g)}$ are functions of the prior private release history and may therefore be statistically dependent on previous Gaussian noise terms. Thus, the decomposition should not be interpreted as an independence, orthogonality, or denoising decomposition.*

Remark 4 (Inherited noise). *SMA-DP-SGD does not explicitly denoise previous private releases. The memory branch is constructed from already-private noisy quantities, so it may contain both inherited recursive signal and inherited Gaussian noise.*

B.9 Interpretation of Spectral Tempering and Private-History Gating

This subsection records structural properties of the spectral and memory controls.

Proposition 3 (Spectral deviation increases tempering). *For*

$$\lambda_t^{(g)}(I_\rho) = 1 - \exp\left(-c_\lambda d_t^{(g)}(I_\rho)\right), \quad c_\lambda > 0,$$

the tempering coefficient $\lambda_t^{(g)}(I_\rho)$ is nondecreasing in the spectral deviation $d_t^{(g)}(I_\rho)$.

Proof. Differentiating gives

$$\frac{\partial \lambda_t^{(g)}(I_\rho)}{\partial d_t^{(g)}(I_\rho)} = c_\lambda \exp\left(-c_\lambda d_t^{(g)}(I_\rho)\right) \geq 0.$$

Hence larger spectral deviation yields larger or equal tempering. \square

Proposition 4 (Larger tempering suppresses older lags). *For fixed shared fractional order $\alpha \in (0, 1]$ and lag $j \geq 1$, the raw memory coefficient*

$$a_{t,j}^{(g)} = (j+1)^{\alpha-1} \exp\left(-\lambda_t^{(g)}(I_\rho)j\right)$$

is nonincreasing in $\lambda_t^{(g)}(I_\rho)$. Moreover, for $j > k$, the ratio $a_{t,j}^{(g)}/a_{t,k}^{(g)}$ decreases as $\lambda_t^{(g)}(I_\rho)$ increases.

Proof. For fixed j ,

$$\frac{\partial a_{t,j}^{(g)}}{\partial \lambda_t^{(g)}(I_\rho)} = -j a_{t,j}^{(g)} \leq 0.$$

For $j > k$,

$$\frac{a_{t,j}^{(g)}}{a_{t,k}^{(g)}} = \left(\frac{j+1}{k+1}\right)^{\alpha-1} \exp\left(-\lambda_t^{(g)}(I_\rho)(j-k)\right),$$

which decreases in $\lambda_t^{(g)}(I_\rho)$ because $j-k > 0$. \square

Proposition 5 (Role of the shared fractional order). *The shared fractional order $\alpha \in (0, 1]$ controls the power-law factor*

$$(j+1)^{\alpha-1}.$$

If $0 < \alpha < 1$, this factor decreases with j . If $\alpha = 1$, the power-law factor is constant and lag dependence is governed only by exponential tempering.

Proof. When $0 < \alpha < 1$, the exponent $\alpha-1$ is negative, so $(j+1)^{\alpha-1}$ decreases as j grows. When $\alpha = 1$, $(j+1)^{\alpha-1} = 1$. \square

Proposition 6 (Bounded private-history alignment gate). *The private-history alignment gate satisfies*

$$0 \leq \Gamma_t^{(g)} \leq 1. \tag{32}$$

Proof. By definition,

$$\Gamma_t^{(g)} = \max \left(0, \frac{\langle \mu_{t-1}^{(g)}, \nu_{t-1}^{(g)} \rangle}{\|\mu_{t-1}^{(g)}\|_2 \|\nu_{t-1}^{(g)}\|_2 + \epsilon} \right).$$

The maximum with zero gives nonnegativity. By Cauchy–Schwarz,

$$\langle \mu_{t-1}^{(g)}, \nu_{t-1}^{(g)} \rangle \leq \|\mu_{t-1}^{(g)}\|_2 \|\nu_{t-1}^{(g)}\|_2.$$

Since $\epsilon > 0$, the denominator is at least $\|\mu_{t-1}^{(g)}\|_2 \|\nu_{t-1}^{(g)}\|_2$. Hence the cosine-like ratio is at most one, and therefore $\Gamma_t^{(g)} \leq 1$. \square

Proposition 7 (Bounded norm scale). *The norm scale satisfies*

$$0 \leq \Psi_t^{(g)} \leq \xi_{\max}. \quad (33)$$

Proof. By definition,

$$\Psi_t^{(g)} = \min \left(\xi_{\max}, \frac{\|\mu_{t-1}^{(g)}\|_2}{\|\nu_{t-1}^{(g)}\|_2 + \epsilon} \right).$$

Both arguments of the minimum are nonnegative, and the first argument is ξ_{\max} . Hence $0 \leq \Psi_t^{(g)} \leq \xi_{\max}$. \square

Proposition 8 (Effect of β). *The fixed mixing coefficient $\beta \in (0, 1]$ creates a direct tradeoff: smaller β reduces the current-step conditional sensitivity bound linearly, but also attenuates the direct current clipped-sum signal by the same factor and increases reliance on the memory branch.*

Proof. By Theorem 1,

$$\Delta_r^{(g)} \leq \beta C^{(g)}.$$

Thus decreasing β reduces the group-wise conditional sensitivity bound linearly. On the other hand,

$$r_t^{(g)} = \beta s_t^{(g)} + b_t^{(g)}(\mathcal{H}_t),$$

so the direct coefficient of the current clipped sum is exactly β . Therefore, decreasing β also weakens the direct current-gradient signal and increases the relative role of the memory branch. \square

Remark 5 (No free privacy improvement). *A smaller β changes the mechanism: it reduces current-query sensitivity, but it also attenuates the current clipped-sum signal and increases dependence on previous private releases. Thus, the privacy effect of β should be interpreted jointly with its optimization effect.*

B.10 Special Cases and Limiting Regimes

Proposition 9 (Exact reduction to group-wise DP-SGD). *If $\beta = 1$, then the memory branch vanishes and SMA-DP-SGD reduces exactly to group-wise DP-SGD:*

$$r_t^{(g)} = s_t^{(g)}, \quad \tilde{s}_t^{(g)} = s_t^{(g)} + \mathcal{N} \left(0, \sigma_{t,g}^2 (C^{(g)})^2 I_g \right).$$

Proof. If $\beta = 1$, then $1 - \beta = 0$. Hence

$$b_t^{(g)}(\mathcal{H}_t) = (1 - \beta) \omega_t \Gamma_t^{(g)} \Psi_t^{(g)} \nu_{t-1}^{(g)} = 0.$$

Therefore $r_t^{(g)} = s_t^{(g)}$, and substituting this into the release rule gives the group-wise DP-SGD Gaussian release. \square

Proposition 10 (No-memory window). *If $K = 1$, then $M_t = 0$ for all t , so*

$$\nu_{t-1}^{(g)} = 0.$$

The memory branch for group g therefore vanishes.

Proof. Since $M_t = \min(K - 1, t)$, setting $K = 1$ gives $M_t = 0$ for all t . By definition, the memory state is zero when no lagged terms are available. \square

Proposition 11 (Warm-up or alignment removal of memory). *If $\omega_t = 0$ or $\Gamma_t^{(g)} = 0$, then the memory branch vanishes for group g at step t .*

Proof. The memory branch is

$$b_t^{(g)}(\mathcal{H}_t) = (1 - \beta)\omega_t\Gamma_t^{(g)}\Psi_t^{(g)}\nu_{t-1}^{(g)}.$$

If either $\omega_t = 0$ or $\Gamma_t^{(g)} = 0$, the product is zero. \square

Proposition 12 (Raw fractional memory). *If $\lambda_t^{(g)}(I_\rho) = 0$, then*

$$a_{t,j}^{(g)} = (j + 1)^{\alpha-1}.$$

Thus the memory kernel reduces to a raw fractional power-law kernel before normalization.

Proof. Substitute $\lambda_t^{(g)}(I_\rho) = 0$ into

$$a_{t,j}^{(g)} = (j + 1)^{\alpha-1} \exp(-\lambda_t^{(g)}(I_\rho)j).$$

The exponential factor becomes one. \square

Proposition 13 (No fractional power-law factor). *If $\alpha = 1$, then*

$$a_{t,j}^{(g)} = \exp(-\lambda_t^{(g)}(I_\rho)j).$$

Thus the fractional power-law factor disappears.

Proof. If $\alpha = 1$, then $(j + 1)^{\alpha-1} = (j + 1)^0 = 1$. \square

Proposition 14 (Uniform memory weights). *If $\lambda_t^{(g)}(I_\rho) = 0$ and $\alpha = 1$, then*

$$a_{t,j}^{(g)} = 1$$

for every active lag j . After normalization,

$$\hat{a}_{t,j}^{(g)} = \frac{1}{M_t}, \quad j = 1, \dots, M_t.$$

Proof. Under $\lambda_t^{(g)}(I_\rho) = 0$ and $\alpha = 1$,

$$a_{t,j}^{(g)} = (j + 1)^0 \exp(0) = 1.$$

The sum of the M_t active raw weights is M_t , so normalization gives $\hat{a}_{t,j}^{(g)} = 1/M_t$. \square

NeurIPS Paper Checklist

1. Claims

Question: Do the main claims made in the abstract and introduction accurately reflect the paper’s contributions and scope?

Answer: [Yes].

Justification: The claims in the abstract and introduction are restricted to the proposed SMA-DP-SGD mechanism, its private-release-history fractional memory design, its WeightWatcher-inspired spectral tempering mechanism, its conditional sensitivity structure, and the empirical privacy–utility behavior observed in the reported experiments. These claims are supported by the methodology in Section 3, the experiments in Section 4, the additional results in Appendix A, and the theoretical analysis in Appendix B.

2. Limitations

Question: Does the paper discuss the limitations of the work performed by the authors?

Answer: [Yes].

Justification: Section 5 discusses limitations including inherited noise from previous private releases, the heuristic nature of the spectral reliability interval, the additional computational overhead introduced by spectral diagnostics and memory computations, and the distinction between marginal privacy-cost diagnostics and formal full-step privacy accounting.

3. Theory assumptions and proofs

Question: For each theoretical result, does the paper provide the full set of assumptions and a complete and correct proof?

Answer: [Yes].

Justification: Appendix B states the theoretical assumptions and provides the formal analysis of SMA-DP-SGD. It includes add/remove adjacency, Poisson subsampling, group-wise clipping, private-release-history conditioning, recursive-query sensitivity, conservative joint RDP accounting, adaptive composition, signal–memory–noise decomposition, parameter interpretations, and limiting regimes.

4. Experimental result reproducibility

Question: Does the paper fully disclose all the information needed to reproduce the main experimental results of the paper to the extent that it affects the main claims and/or conclusions of the paper, regardless of whether the code and data are provided or not?

Answer: [Yes].

Justification: Appendix A.1 provides the experimental setup and reproducibility details, including datasets, baselines, group-wise/layer-wise parameter grouping, SMA-DP-SGD configuration, repeated-run reporting, and hyperparameters specific to the proposed method. The main experimental results are reported in Section 4, with additional statistics and diagnostics in Appendix A.

5. Open access to data and code

Question: Does the paper provide open access to the data and code, with sufficient instructions to faithfully reproduce the main experimental results, as described in supplemental material?

Answer: [No].

Justification: The paper uses standard publicly available benchmark datasets, including CIFAR-100, CIFAR-10, and MNIST, and provides methodological and experimental details in Section 3, Section 4, and Appendix A.1. The source code is not released at submission time. If the paper is published, we plan to provide the implementation and scripts upon reasonable request to support reproduction of the reported results.

6. Experimental setting/details

Question: Does the paper specify all the training and test details, e.g., data splits, hyperparameters, how they were chosen, type of optimizer, necessary to understand the results?

Answer: [Yes].

Justification: The experimental setting is summarized in Section 4 and described in detail in Appendix A.1. The paper specifies the datasets, baselines, layer-wise instantiation of parameter groups, shared fractional order, shared memory window, fixed mixing coefficient, spectral reliability interval, tempering constant, repeated-run protocol, and statistical reporting. Additional ablation and diagnostic results are provided in Appendix A.

7. Experiment statistical significance

Question: Does the paper report error bars suitably and correctly defined or other appropriate information about the statistical significance of the experiments?

Answer: [Yes].

Justification: Appendix A.4 reports final CIFAR-10 accuracy over three independent runs using mean, sample standard deviation, and two-sided 95% confidence intervals computed using the Student- t interval. This provides statistical information about run-to-run variability for the final accuracy comparison.

8. Experiments compute resources

Question: For each experiment, does the paper provide sufficient information on the computer resources, type of compute workers, memory, time of execution, needed to reproduce the experiments?

Answer: [Yes].

Justification: Runtime and relative computational overhead are reported in Appendix A.7. The reproducibility description in Appendix A.1 states that runtime is measured under the same hardware and software environment for all optimizers in the runtime comparison. The paper reports the relative overhead of SMA-DP-SGD compared with DP-SGD and other DP baselines.

9. Code of ethics

Question: Does the research conducted in the paper conform, in every respect, with the NeurIPS Code of Ethics <https://neurips.cc/public/EthicsGuidelines>?

Answer: [Yes].

Justification: The work is methodological and experimental. It uses public benchmark datasets and does not involve human subjects, private user data, deceptive systems, high-risk deployment, or released high-risk models. Privacy-related assumptions, limitations, and responsible-use considerations are discussed in Section 5 and Section 6.

10. Broader impacts

Question: Does the paper discuss both potential positive societal impacts and negative societal impacts of the work performed?

Answer: [Yes].

Justification: Section 6 discusses the potential positive impact of improving utility in differentially private learning for sensitive domains, as well as risks associated with incorrect privacy accounting, inappropriate privacy-budget interpretation, computational overhead, and deployment in high-stakes applications.

11. Safeguards

Question: Does the paper describe safeguards that have been put in place for responsible release of data or models that have a high risk for misuse, e.g., pre-trained language models, image generators, or scraped datasets?

Answer: [N/A].

Justification: The paper does not release high-risk pretrained models, language models, image generators, scraped datasets, or dual-use datasets. The experiments use standard public benchmark datasets and focus on a differentially private optimization method.

12. Licenses for existing assets

Question: Are the creators or original owners of assets, e.g., code, data, models, used in the paper, properly credited and are the license and terms of use explicitly mentioned and properly respected?

Answer: [Yes].

Justification: The paper uses standard public benchmark datasets and standard software tools for machine learning experiments. The relevant datasets and prior methods are cited in the paper. No proprietary, restricted, or newly scraped datasets are introduced.

13. New assets

Question: Are new assets introduced in the paper well documented and is the documentation provided alongside the assets?

Answer: [N/A].

Justification: The paper does not introduce or release a new dataset, benchmark, pretrained model, or standalone software asset at submission time. The contribution is a private optimization method. The algorithmic details are documented in Section 3, and additional experimental and theoretical details are provided in Appendix A and Appendix B.

14. Crowdsourcing and research with human subjects

Question: For crowdsourcing experiments and research with human subjects, does the paper include the full text of instructions given to participants and screenshots, if applicable, as well as details about compensation, if any?

Answer: [N/A].

Justification: The paper does not involve crowdsourcing, user studies, surveys, annotation tasks, or research with human subjects. All experiments are conducted on public machine-learning benchmark datasets.

15. Institutional review board (IRB) approvals or equivalent for research with human subjects

Question: Does the paper describe potential risks incurred by study participants, whether such risks were disclosed to the subjects, and whether Institutional Review Board approvals, or an equivalent approval/review based on the requirements of your country or institution, were obtained?

Answer: [N/A].

Justification: The paper does not involve human subjects, crowdsourcing, private participant data, user studies, or human-subject interventions; therefore IRB approval or equivalent human-subjects review is not applicable.

16. Declaration of LLM usage

Question: Does the paper describe the usage of LLMs if it is an important, original, or non-standard component of the core methods in this research? Note that if the LLM is used only for writing, editing, or formatting purposes and does *not* impact the core methodology, scientific rigor, or originality of the research, declaration is not required.

Answer: [N/A].

Justification: LLMs are not used as an important, original, or non-standard component of the proposed method, theoretical analysis, experiments, or evaluation. Any use of language tools, if applicable, is limited to writing, editing, or formatting assistance and does not affect the scientific content or core methodology.